



TALLINN UNIVERSITY OF TECHNOLOGY
SCHOOL OF ENGINEERING
Department of Material and Environmental Technology

ANTIMONY SELENIDE THIN FILMS BY CATION EXCHANGE

ANTIMOONSELENIIDI ÕHUKESTE KILEDE SÜNTEES KATIOONIVAHETUSE MEETODIL

MASTER THESIS

Student: Tatiana Vaarik

Student code: 201636KAYM

Supervisor: Dr. Olga Volobujeva, Senior Research Scientist

Dr. Svetlana Polivtseva, Researcher

Tallinn 2023

AUTHOR'S DECLARATION

Hereby I declare, that I have written this thesis independently.

No academic degree has been applied for based on this material. All works, major viewpoints and data of the other authors used in this thesis have been referenced.

"....." January 2023

Author:

/signature /

Thesis is in accordance with terms and requirements

"....." January 2023.

Supervisor:

/signature/

Accepted for defence

"....." January 2023

Chairman of theses defence commission:

/name and signature/

Non-exclusive licence for reproduction and publication of a graduation thesis¹

I, Tatiana Vaarik,

1. grant Tallinn University of Technology free licence (non-exclusive licence) for my thesis

Antimony selenide thin films by cation exchange,

supervised by Dr. Olga Volobujeva and Dr. Svetlana Polivtseva,

1.1 to be reproduced for the purposes of preservation and electronic publication of the graduation thesis, incl. to be entered in the digital collection of the library of Tallinn University of Technology until expiry of the term of copyright;

1.2 to be published via the web of Tallinn University of Technology, incl. to be entered in the digital collection of the library of Tallinn University of Technology until expiry of the term of copyright.

2. I am aware that the author also retains the rights specified in clause 1 of the non-exclusive licence.

3. I confirm that granting the non-exclusive licence does not infringe other persons' intellectual property rights, the rights arising from the Personal Data Protection Act or rights arising from other legislation.

12.01.2023

¹ *The non-exclusive licence is not valid during the validity of access restriction indicated in the student's application for restriction on access to the graduation thesis that has been signed by the school's dean, except in case of the university's right to reproduce the thesis for preservation purposes only. If a graduation thesis is based on the joint creative activity of two or more persons and the co-author(s) has/have not granted, by the set deadline, the student defending his/her graduation thesis consent to reproduce and publish the graduation thesis in compliance with clauses 1.1 and 1.2 of the non-exclusive licence, the non-exclusive license shall not be valid for the period.*

Department of Material and Environmental Technology

THESIS TASK

Student: Tatiana Vaarik, 201636KAYM

Study programme: KAYM - Materials and Processes for Sustainable Energetics

main speciality: Materials for sustainable energetics

Supervisor(s): Senior Research Scientist, Dr. Olga Volobujeva, +3726203368

Researcher, Dr. Svetlana Polivtseva, +3726203368

Thesis topic:

Antimony selenide thin films by cation exchange

Antimoonseleeniidi õhukeste kilede süntees katioonivahetuse meetodil

Thesis main objectives:

1. To investigate the applicability of cation exchange to invert SnSe thin films into Sb₂Se₃ thin films
2. To study the effect of reducing SbCl₃ concentration on the cation exchange process
3. To study the effect of time treatment on the cation exchange process

Thesis tasks and time schedule:

No	Task description	Deadline
1.	Preliminary experiments to find the right conditions for conducting Sn-to-Sb inversion by cation exchange	
2.	Conducting experiments with reducing SbCl ₃ concentration	
3.	Performing experiments to investigate the effect of time treatment on the cation exchange process	
4.	Characterisation of the treated samples by HR-SEM/EDX, XRD, Raman and UV-vis spectroscopy	

Language: English **Deadline for submission of thesis:** "12" January 2023

Student: Tatiana Vaarik "12" January 2023

/signature/

Supervisor: Dr. Olga Volobujeva "" January 2023

/signature/

Co-supervisor: Dr. Svetlana Polivtseva "" January 2023

/signature/

Head of study programme: Dr. Sergei Bereznev "" January 2023

/signature/

CONTENTS

PREFACE.....	6
List of abbreviations and symbols.....	7
INTRODUCTION.....	8
1. LITERATURE OVERVIEW.....	10
1.1. Antimony selenide (Sb_2Se_3).....	10
1.1.1. Phase diagram and Sb_2Se_3 crystal structure.....	10
1.2. Industrial deposition methods.....	12
1.2.1. Thermal evaporation.....	12
1.2.2. Close-space sublimation.....	14
1.2.3. Magnetron sputtering.....	15
1.2.4. Chemical bath deposition.....	16
1.2.5. Chemical spray pyrolysis.....	18
1.2.6. Atomic layer deposition.....	19
1.3. Applicability of Sb_2Se_3 thin films.....	20
1.4. Cation exchange.....	22
1.4.1. Formation of cation exchanged materials.....	22
1.5. Summary and aim of thesis.....	24
2. EXPERIMENTAL PART.....	25
2.1. Tin (II) Selenide deposition.....	25
2.2. Sn-to-Sb replacement.....	25
2.3. Characterisation.....	26
3. RESULTS AND DISCUSSION.....	28
3.1. Preliminary experiments.....	28
3.2. Effect of reducing SbCl_3 concentration.....	29
3.3. Effect of time treatment.....	32
4. CONCLUSIONS.....	36
SUMMARY.....	38
LIST OF REFERENCES.....	39

PREFACE

The topic of this thesis was initiated by my supervisors Dr. Olga Volobujeva and Dr. Svetlana Polivtseva. The research was mainly carried out in the Laboratory of Photovoltaic Materials of Tallinn University of Technology.

I would like to express my gratitude to my supervisors Dr. Olga Volobujeva and Dr. Svetlana Polivtseva for their support on the way to thesis defence. Without their vital advice and vigilance, I would have never reached the finishing line of the studies. I am grateful to Professor Sergei Bereznev for his caring and advising attitude towards his students. Additionally, I would like to thank Tallinn University of Technology for giving me the opportunity to study here and all the personnel of the university who I encountered throughout studies for their help, patience and assistance.

This work was aimed on testing the applicability of cation exchange to invert continuous SnSe thin films into Sb_2Se_3 thin films attached to the substrate. SnSe thin films used as matrices in the cation exchange process were deposited onto various substrates at different temperatures using magnetron sputtering. The cation exchange process was carried out at 210 °C in the SbCl_3 solutions of different solvents, concentrations and time treatments. Glycerol was found to be the most suitable solvent for the treatment. Different characterisation techniques were applied to characterise formed films. It was concluded that substrate type, SbCl_3 solution molarity and time treatment were the critical parameters for the cation exchange process. SnSe thin films deposited onto a glass substrate peeled off regardless SbCl_3 solution concentrations and time treatment used. SnSe films deposited at temperatures above 300 °C onto Mo, FTO, ITO withstood cation exchange at concentrations below 45 mM. The SbCl_3 solution concentrations between 11 and 45 mM induced the SnSe-to- Sb_2Se_3 full transformation. Time treatments exceeding 5 min induced the SnSe-to- Sb_2Se_3 conversion. Further time treatment raise increased Sb content in the films. Time treatments of 17 and 22 min in 44 mM solution led to the full inversion of SnSe thin films into Sb_2Se_3 . Formed Sb_2Se_3 thin films exhibited orthorhombic Sb_2Se_3 crystals oriented along (hk1) planes, stoichiometric Sb/Se atomic ratio and a direct optical band gap of 1.28 eV.

Keywords: chemical transformation, Sb_2Se_3 , thin films, ion exchange, master thesis

List of abbreviations and symbols

ALD	Atomic layer deposition
CBD	Chemical bath deposition
CSP	Chemical spray pyrolysis
CSS	Close-space sublimation
EDX	Energy dispersive X-ray
J_{sc}	Short circuit current
PCE	Power conversion efficiency
PEC	Photoelectrical cell
PV	Photovoltaic
RF	Radio frequency
RT	Room temperature
SEM	Scanning electron microscope
TE	Thermal evaporation
UV-vis	Ultraviolet-visible
V_{oc}	Open circuit voltage
XRD	X-ray diffraction spectroscopy

INTRODUCTION

The humanity is very dependent on energy sources, and fossil fuels are one of the main supplies of energy in nowadays world [1]. However, as a recurring energy crisis hits the world due to fossil fuels scarce and limited availability of them, alternative energy sources play a key role in providing the needs in the future. Besides a limited amount of available fossil fuel sources, the burning of those causes CO₂-emission and, thus, the greenhouse effect leading to increase in the planet temperature and other harmful effects. Many countries have already changed their policies in the CO₂-emission regulations with support towards renewable energy [2]. Thus, the development of photovoltaics materials is under particular interest.

Currently, solar cells are divided into several generations [3]. First generation of PVs is wafer-based monocrystalline and polycrystalline silicon. This type is the most prevalent on the market due to its relatively high efficiency, Si-abundance, and non-toxicity, but the cost of production is comparably high since silicon crystals are produced at temperatures above 1000 °C. Second generation are thin film solar cells which include CdTe- and CuInGaSe₂-based thin films. Cd is a toxic compound and Te, In and Ga are high-priced elements, and, thus, it limits their wide applicability. Third generation is dye-sensitized solar cells, perovskite, concentrated solar cells, multijunction solar cells. These are emerging technologies yet and have difficulties in applicability which restrict their use, and due to that they are not commercially available yet [3].

Focusing on the second generation of solar cells, the need to replace the existing absorber materials has emerged owing to their cost and toxicity, and one of the perspective substitutes is antimony (III) selenide [4].

Antimony selenide is an absorber material which is being currently thoroughly studied to substitute thin films made of Cu(In,Ga)Se₂ and CdTe due to In- and Ga- scarcity (therefore, high cost) and Cd toxicity. Sb₂Se₃ is a convenient alternative as it is a stable, environmentally friendly, earth crust abundant and, thus, affordable alternative.

Antimony selenide is considered as a material with low toxicity as it is not presented on the list of highly toxic and carcinogenic materials by Chinese, American and European Union regulation authorities [5]. In addition to it, antimony selenide lethal dosage is not mentioned in LD50 nor LCT50. Sb and Se abundance of 0.2 and 0.05 ppm, respectively, in the Earth's crust are higher in comparison with those of In and Te - 0.049 ppm and 0.005 ppm, respectively [5].

Current work is focused on testing applicability of cation exchange to transform a given thin films into Sb_2Se_3 thin films as an alternative way to synthesise semiconductor materials. No previous reports have ever covered cation exchange with transforming thin films into Sb_2Se_3 .

This work has the next organisation:

- Chapter 1 – gives a theoretical background on antimony selenide and its properties, physical and chemical Sb_2Se_3 deposition methods with the review on the deposited Sb_2Se_3 thin films with perspective applicability of Sb_2Se_3 thin films and a brief overview of cation exchange mechanism with brief outlook on the selenides obtained by it.
- Chapter 2 – describes the experimental procedure and means of investigation.
- Chapter 3 – demonstrates the results of the investigation and efforts of discussing them.
- Chapter 4 – concludes and summarises the results of the study.

1. LITERATURE OVERVIEW

1.1. Antimony selenide (Sb_2Se_3)

1.1.1. Phase diagram and Sb_2Se_3 crystal structure

Antimony (Sb) is a chemical element of a group 15 in the Periodic Table, exhibiting various oxidation states including -3, 0, +3, and +5 [6]. Most common and stable oxidation states of antimony in the environment are trivalent (III) and pentavalent (V) [7]. Depending on the surrounding atoms, Sb(III) or Sb(V) can be stabilised. Selenium seems to stabilise the trivalent oxidation state leading to the formation of antimony selenide Sb_2Se_3 [7]. Antimony (III) selenide is a semiconductor displaying attractive thermoelectric and optoelectronic properties [8].

The Sb-Se phase diagram (Figure 1) presents Sb_2Se_3 comprising ~ 40 at. % of Sb as the only existing thermodynamically stable phase in Sb-Se system [9]. To date, no other polymorphic modification of Sb_2Se_3 has been reported. The formation of numerous antimony selenide compounds with different stoichiometry such as SbSe , Sb_2Se_n ($n=2\text{...}4$), Sb_4Se_n ($n=3,4$), Sb_3Se_n ($n=1\text{...}4$) and Sb_4Se_n ($n=3, 4$) [10–13], has been only recorded in gaseous phases as decomposition products of Sb_2Se_3 , and, thus, they are not included in the diagram in Figure 1. The Sb-Se phase diagram includes 4 phases: liquid, solid Sb, solid Se and crystalline orthorhombic Sb_2Se_3 [14].

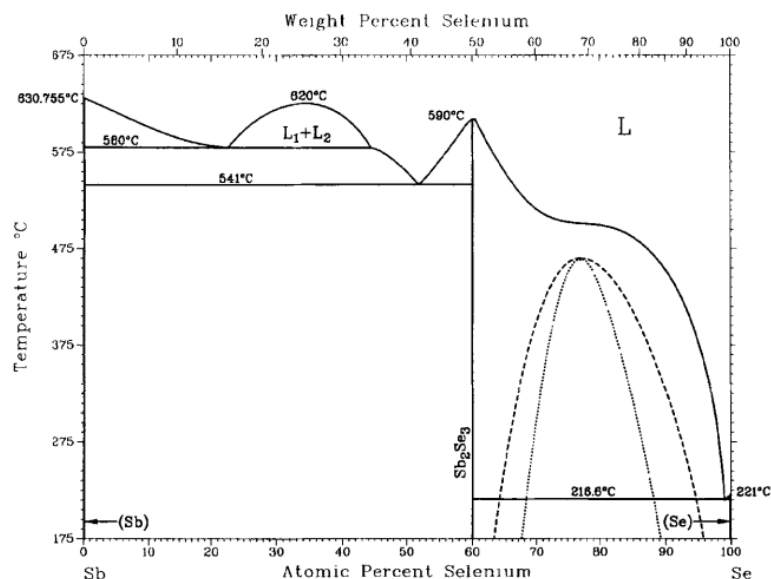
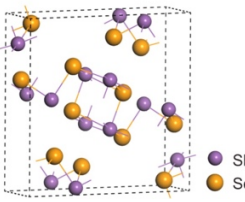
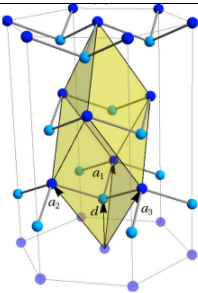
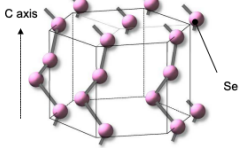
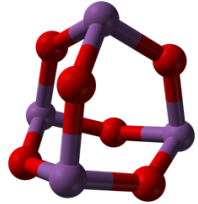
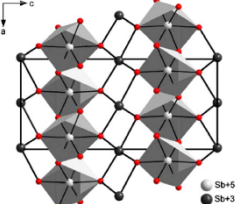


Figure 1. Phase diagram of Sb-Se [9].

Depending on synthetic protocols applied, materials from the antimony selenide system could contain different secondary phases briefly tabulated in Table 1.

Table 1. Stable modifications of Sb_2Se_3 and typical secondary phases presented in antimony selenide materials.

Compound	Lattice parameters	Conditions	Crystal structure	Ref
	Unit cell type		Space group	
Sb_2Se_3	a=11.620 Å b=11.770 Å c=3.629 Å	Orthorhombic Sb_2Se_3 contains 40 at. % of Sb and exists below 611 °C.		[5,9, 14–16]
	Orthorhombic		Pnma	
Sb	a=b=4.308 Å c=11.274 Å	Stable at temperatures below 630 °C.		[17]
	Hexagonal		$R\bar{3}m$	
Se	a=b=4.366 Å c=4.954 Å	Stable under ambient conditions.		[18, 19]
	Hexagonal		$P3_121$	
Sb_2O_3	a=b=c=11.152 Å	Contains 40 at. % of Sb and stable below 570°C.		[20, 21]
	Cubic		$Fd\bar{3}m$	
$\alpha\text{-Sb}_2\text{O}_4$	a=5.443 Å b=4.810 Å c=11.783 Å	Thermodynamically stable below 935°C.		[22]
	Orthorhombic		Pna21	

There is no agreement in the literature about the transition type for Sb_2Se_3 , being direct or indirect. Some authors determined direct bandgap values ranging from 1.2 to 1.3 eV [23, 24]. Others advocated that Sb_2Se_3 is a semiconductor with an indirect bandgap of about 1.1 eV [16, 25].

Researchers have no consistency in the conductivity type observed for antimony selenide materials. In general, single phase Sb_2Se_3 might exhibit p-type behaviour originating from antimony vacancies or external dopant [26]. Few studies reported the formation of n-type Sb_2Se_3 depending on stoichiometry, secondary phases and/or extrinsic doping [27].

Thus, orthorhombic Sb_2Se_3 is the only thermodynamically stable form existing in the Sb-Se system and can exhibit tailorable optical and electrical properties depending on synthetic procedure to be employed.

1.2. Industrial deposition methods

Considering the phase diagram of Sb_2Se_3 in Figure 1, synthesis can be performed using physical or chemical deposition methods. Most widely used physical techniques for the formation of Sb_2Se_3 thin films are represented by thermal evaporation TE [25, 28], close space sublimation CSS [29, 30], and magnetron sputtering [31, 32]. Atomic layer deposition ALD [33], chemical spray pyrolysis CSP [34, 35], and chemical bath deposition CBD [36] represent the family of chemical methods with a commercial potential.

Physical methods

1.2.1. Thermal evaporation

Thermal evaporation is one of the widely employed method to deposit different thin film materials [37–39] In this method, the vapours of the material formed upon heating condense on the cold substrates in a vacuum chamber. A low pressure of about 10^{-6} Torr is typically used to minimize the interaction between the generated vapours and atmosphere [37]. Schematic illustration of the thermal evaporation systems is shown in Figure 2.

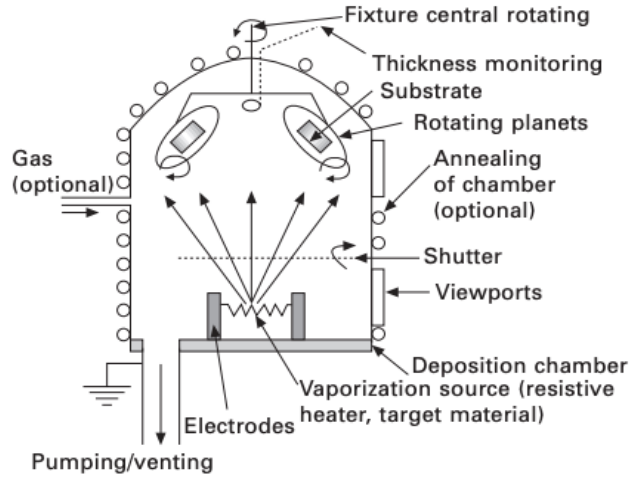
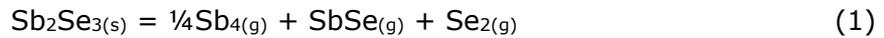


Figure 2. Schematic illustration of thermal evaporation system [38].

Negative formation enthalpy ($\Delta H_f = -30$ kcal/mol) [40] and high vapor pressure (22 Pa at 400 °C) facilitate the formation of antimony (III) selenide by physical methods [8]. However, possible decomposition according to equation 1 during physical formation of Sb_2Se_3 in the temperature region of 400-550 °C can complicate the growth of phase-pure materials [41].



Liu, et al. have synthesized Sb_2Se_3 thin films by TE at different deposition temperatures [28]. Films formed below 150 °C were amorphous with poor adhesion to the substrate. Films deposited at 290 °C were polycrystalline and consisted of orthorhombic Sb_2Se_3 as a main crystalline phase with no preferred orientation. Irrespective of substrate temperature used for the condensation, all films contained antimony oxide Sb_2O_3 secondary phase, most probably formed during the synthesis as a relatively high pressure of $\sim 10^{-3}$ Pa was used in a chamber or later upon oxidation when films were exposed to air [28].

It has been found that substrate temperature is one of the key parameters to control the preferred orientation of thermally evaporated Sb_2Se_3 films [25, 28]. Deposition performed below 250 °C and above 350 °C leads to unfavourable [hk0] orientations in Sb_2Se_3 , while the temperatures lying between them dominate crystallization along [hk1] planes. In general, the growth along [hk1] planes that corresponds to $(\text{Sb}_4\text{Se}_6)_n$ ribbons perpendicularly aligned to the substrate is preferable over the [hk0] orientations, as it improves the carrier transport mechanism in the absorber (Figure 3). On the other hand, dominant formation of [hk0] planes with grains stacked horizontally on the substrate harms the parameters of optoelectronic devices [25, 28].

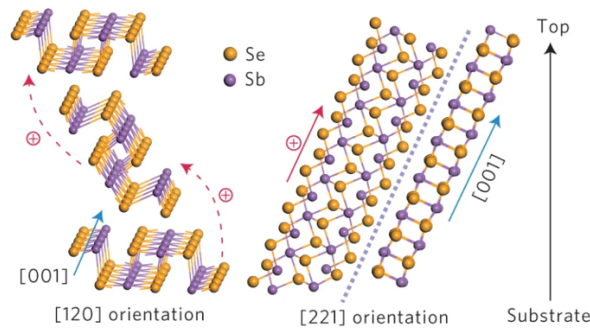


Figure 3. Orientation of Sb_2Se_3 crystal growth [42]. $[\text{hk}0]$ is unfavourable, $[\text{hk}1]$ is preferred. When excited, charge carriers will have to jump from-ribbon-to-ribbon in $[\text{hk}0]$ oriented crystal (the charge carrier hop is marked with red dashed line). In $[\text{hk}1]$ directions, charge carriers move freely along the crystal [42].

1.2.2. Close-space sublimation

Close-space sublimation (CSS) is an industrial physical method enabling to form high-quality thin films at low cost and high deposition rate [43]. Figure 4 shows a schematic illustration of CSS setup. In CSS, species vaporized from the source are transported to the closely positioned substrate, forming thin-film materials. Atmosphere, source temperature and substrate temperature can be varied to reach the desired material properties [43, 44].

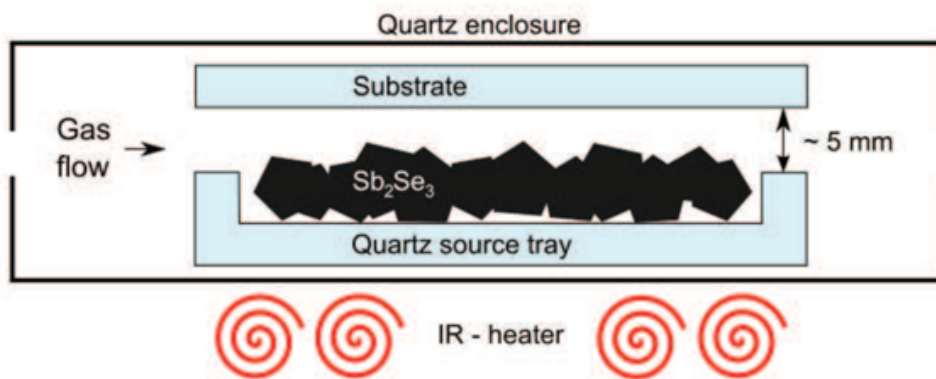


Figure 4. Schematic of the CSS experimental setup [44].

Hutter et al. [45] demonstrated the formation of uniform, pinhole-free, tightly packed Sb_2Se_3 films onto FTO/ TiO_2 substrate using a two-step process consisting of depositing a seed layer at a source temperature of 350 °C and forming main layer at 450 °C.

However, EDX analysis confirmed a strong selenium deficiency of about 4%, indicating the presence of a secondary phase, presumably metallic Sb [45].

Numerous studies have shown that the morphology of the formed Sb_2Se_3 layers and preferred growth along the $[\text{hk}1]$ planes can be controlled in the CSS process by varying the underlying layer and/or deposition temperature [44–46].

1.2.3. Magnetron sputtering

Magnetron sputtering is a third common deposition technique for fabricating different high-quality thin films used in many applications [38, 47–51]. In the sputtering process, ionized gas (usually Ar) ejects atoms from the cathode target, which are deposited on the anode substrate (Figure 5). Changing the sputtering power, operating pressure, target-to-substrate distance, etc. enables adjusting the properties of formed layers [47, 49–51].

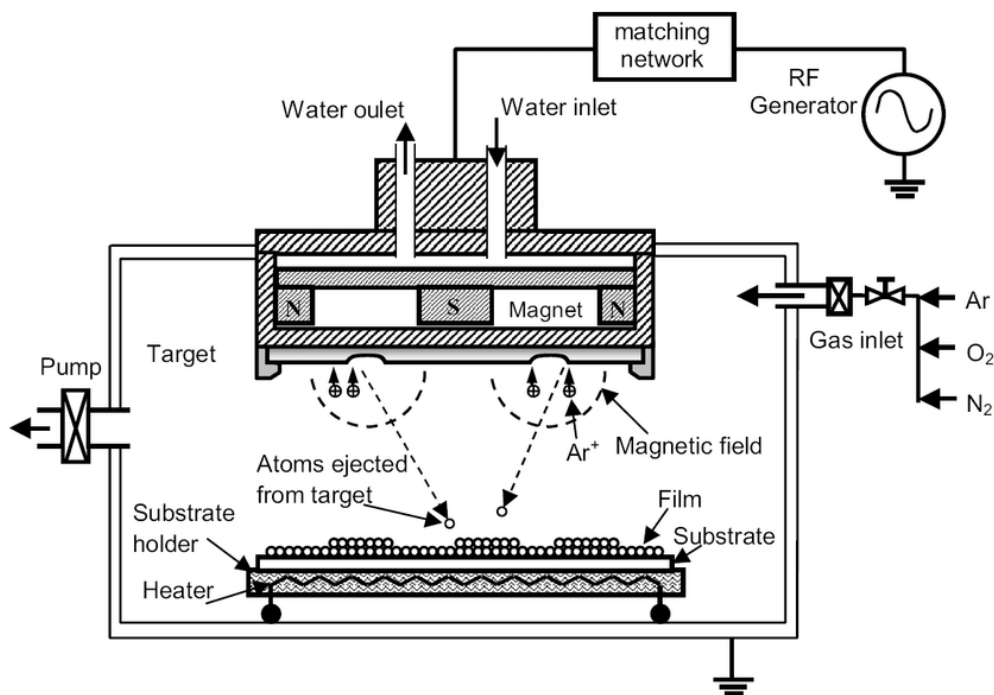


Figure 5. Schematic illustration of magnetron sputtering deposition [52].

G. Spaggiari [53] explored the properties of Sb_2Se_3 films grown by RF sputtering at different substrate temperatures. The films were flat and close to stoichiometric compositions at temperatures below 120 °C. With an increase in the substrate temperature from RT to 330 °C, the direct bandgap values decreased from 1.46 eV to 1.22 eV as more crystalline materials were formed [53].

Near stoichiometric compositions have been demonstrated for almost amorphous Sb_2Se_3 films sputtered only at 200 °C [54]. In the temperature range of 250-400 °C, the formed films crystallized with a high selenium deficiency [54]. A relatively high Se-deficiency of about 3% has been reported even at RT [55].

Chemical methods

1.2.4. Chemical bath deposition

Chemical bath deposition is a well-known chemical method to deposit numerous metal chalcogenide films [56–59], offering simplicity, variability of the starting precursors, cost-effectiveness, and proven scalability for industrial implementation [60]. Typical deposition can be performed using a very simple setup (Figure 6) requiring only a substrate to be placed in a vessel containing necessary precursors and a heater to maintain a suitable temperature for the synthesis [61].

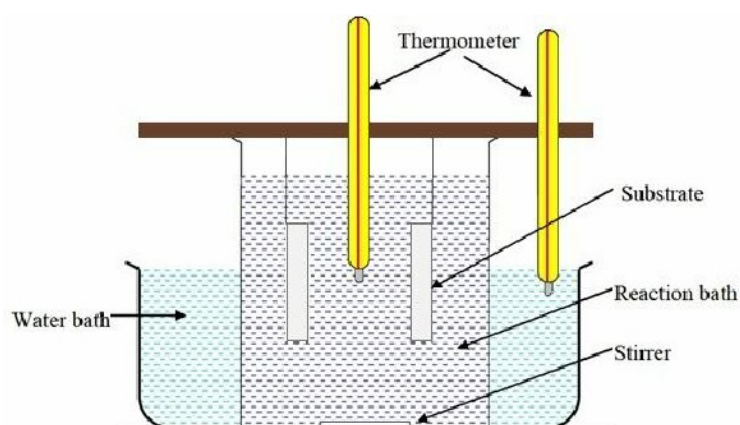


Figure 6. Schematic illustration for CBD setup [62].

The basic principles of CBD are released via several intermediate steps, each of which can contribute to the final properties of synthesized materials [63]:

- Nucleation is characterised by reaching the chemical equilibria in solution and forming an initial monolayer on the substrate surface.
- Growth is defined by intense condensing target ions on top of the initial monolayer acting as a catalyst surface.
- Termination is characterized by a steadily decreasing film growth rate close to reaching the maximum film thickness.

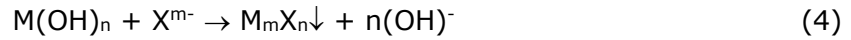
There is no agreement in the literature on the primary mechanism taking place during the CBD process [64]. In general, four main mechanisms can be considered to control the properties of deposited materials [60]:

Ion-by-ion is probably realized during nucleation and can be expressed by equation 2 [60]:



where M^{n+} is a metal cation, X^{m-} is a target anion, and M_mX_n is a reaction product deposited on the substrate.

Cluster hydroxide can determine each synthetic stage being nucleation, growth, and/or termination and be described as equations 3 and 4 [60]:



If the cluster hydroxide mechanism is dominating the process, the formed colloidal hydroxide particles adhere to the substrate and interact with the target anions to form the desired film [60, 65].

Complex decomposition ion-by-ion is determined by the interaction of metal ions with ligands containing groups with the desired X atoms, resulting in the formation of complexes [60]. The latter compounds are later hydrolysed by hydroxyl ions realizing M_mX_n to be deposited on the substrate and other decomposition by-products [60].

Complex decomposition cluster dominates if the realizing M_mX_n occurs during the decomposition of complex compounds formed between hydroxide $M(OH)_n$ and anion-containing complexing agent [60].

Regardless of the mechanism controlling the synthesis, the fabricated films of metal sulphide/selenide can be contaminated by metal hydroxide [66, 67]. To suppress this, a complexing agent is usually introduced into the solution to control the amount of uncomplexed metal. However, even the addition of an appropriate complexing agent limits the ability to eliminate metal oxide/hydroxide presented in layers consisting of metal cations prone to hydrolysis [66, 68].

The formation of amorphous Sb_2Se_3 films has been reported when using solutions containing citrate or tartrate anions and sodium selenosulfate as a selenium source [69].

The obtained films exhibited a strong Se deficiency and contained antimony oxide(hydroxide) as a secondary phase irrespective of the deposition temperature, chemical composition in solution, and duration of the CBD process [69].

Additive-assisted synthesis performed using solutions containing simultaneously selenourea and sodium selenosulfate significantly reduced the content of oxides in the obtained Sb_2Se_3 films [36].

1.2.5. Chemical spray pyrolysis

Chemical spray pyrolysis is a low-cost approach to fabricating materials, offering simplicity in deposition setups (Figure 7), and scalability for deposition over large-area substrates and industrial processes [70]. In CSP, a precursor solution is sprayed onto pre-heated substrates, where solution components are pyrolyzed to form thin films. Properties of the formed films can be controlled by varying different parameters such as substrate temperature, solution composition, carrier gas flow rate, solvent type, etc. [70].

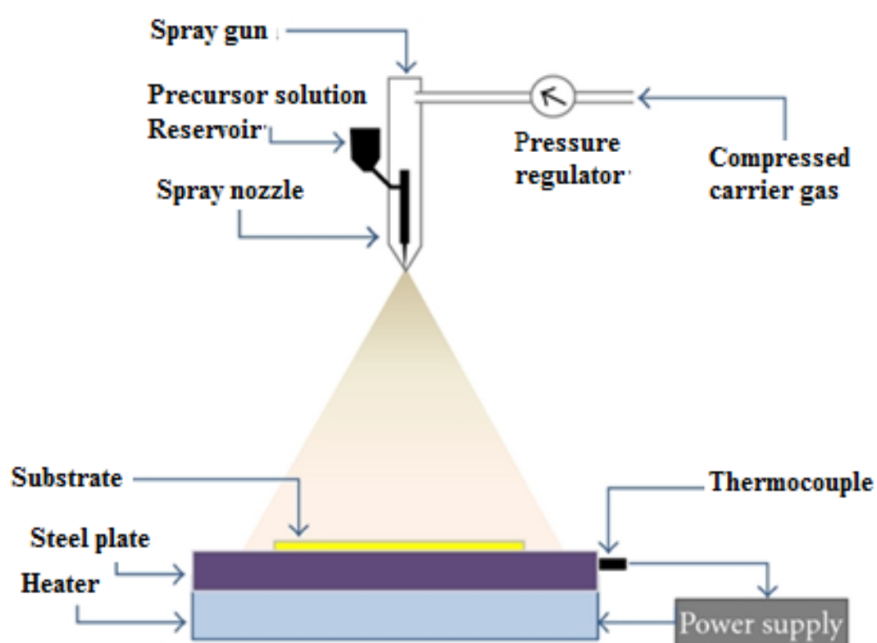


Figure 7. Schematic spray pyrolysis setup [71].

Fabrication of Sb_2Se_3 films by CSP has been reported in [34, 35]. Spraying both aqueous or non-aqueous solutions containing antimony (III) chloride, SeO_2 or selenourea [$CSe(NH_2)_2$] at substrate temperatures of about 300 °C resulted in almost amorphous layers with optical bandgaps of around 1.8-2.0 eV. When spraying solutions contained

tartaric acid as a complexing agent to hinder hydrolysis reactions, films were inhomogeneous with visual contaminations [34, 35].

Beyond the issues with phase composition, the efficient conversion of the initial reactants into a film attached to the substrate (reaction yield) has often been ignored in both CBD and CSP [72, 73]. Low reaction yield is a concern in all industrial processes and is especially important in cases with toxic or extremely expensive precursors.

1.2.6. Atomic layer deposition

Atomic layer deposition relies on complementary reactions between the substrate with a formed layer and precursors supplied by a gaseous phase [74, 75].

Considering the synthesis of Sb_2Se_3 , alternate delivering of Sb^{III} or Se^{II} ions in ALD could offer not only thickness control but also stoichiometric compositions [71]. Deposition performed by ALD at 150 °C using selenium dimethyldithiocarbamate as a selenium source and tris(dimethylamino) antimony as a metal source resulted in the crystalline Sb_2Se_3 film contaminated by small amounts of carbon (C), sulphur (S), and nitrogen (N) [33].

Solution atomic layer deposition sALD carried out at room temperature employing antimony (III) chloride and bis(trimethylsilyl)selenide or numerous n-alkylstannyl selenides as Sb and Se sources, respectively, yielded the formation of amorphous Sb_2Se_3 films with a relatively high oxygen content [76].

One of the main drawbacks of ALD is the limited availability of suitable Se precursors intended for the synthesis of metal selenide materials [76]. The first and seems to be a logical choice as H_2Se complicates the development of thin films due to its high toxicity and low chemical stability. In addition, when using metal chloride as a metal source, the formation of aggressive HCl by-products occurs. Thus, to fully benefit from ALD-grown metal selenides, the elaboration of appropriate selenium sources with sufficient volatility, accompanied by reasonable thermal stability and reactivity, is required [76].

1.3. Applicability of Sb₂Se₃ thin films

Antimony (III) selenide has been considered as an eco-friendly absorber material for different optoelectronic applications due to its bandgap of ~ 1.2 eV, high absorption coefficient, and high charge-carrier mobility [8, 77]. Numerous studies have recently demonstrated the applicability of Sb₂Se₃ in thin-film solar cells (Table 2) [36, 46, 55, 78–85], photoelectrochemical (PEC) water-splitting cells [86], [87], photodetectors [8, 88], and memory devices [8, 89], meeting the requirements for the availability of constituent elements and low-toxicity under the strategy toward a green society.

Table 2. PV characteristics of some champion Sb₂Se₃-based devices fabricated by methods most scalable to the industrial scale.

Method	Solar cell structure	V _{oc} , V	J _{sc} , mA/cm ²	FF, %	PCE, %	Ref.
TE	ITO/CdS/Sb ₂ Se ₃ /Au	0.360	25.3	52.5	4.8	[78]
	ITO/SnO ₂ /CdS/Sb ₂ Se ₃ /Au	0.380	28.1	59.1	6.2	[79]
CSS	FTO/TiO ₂ /Sb ₂ Se ₃ /Au	0.430	24.6	50.0	5.3	[46]
	Mo/Sb ₂ Se ₃ /CdS/IZO/AZO/Ag	0.446	26.4	54.9	6.4	[80]
	FTO/CdS/Sb ₂ Se ₃ /t-Se/Au	0.413	28.9	62.3	7.5	[81]
	Mo/Sb ₂ Se ₃ /CdS/i-ZnO/AZO/Ag	0.505	27.7	60.7	8.5	[82]
	Mo/MoSe ₂ /Sb ₂ Se ₃ /TiO ₂ /CdS/ZnO/ZnO:Al	0.400	32.6	70.3	9.2	[83]
Sputtering	Mo/Sb ₂ Se ₃ /CdS/ITO/Ag	0.494	25.9	47.7	6.1	[55]
	Mo/Sb ₂ Se ₃ /CdS/ITO/Ag	0.504	24.9	54.5	6.8	[84]
	Mo/Sb ₂ Se ₃ /CdS/ITO/Ag	0.520	27.8	59.8	8.6	[85]
CBD	FTO/CdS/Sb ₂ Se ₃ /Spiro-OMeTAD/Au	0.467	33.5	67.6	10.6	[36]

The results of the lab-scale solar cell fabrication (Table 3) with the recent record efficiency of 10.57% [36] clearly indicate a high potential of Sb₂Se₃ to be implemented as an absorber in thin-film structures.

However, to increase the PV parameters closer to theoretically achievable values: V_{oc} of 0.935 V, J_{sc} of 40 mA/cm², FF of 87.7 % and PCE of 32.7 % [90], the phase compositions of synthesized Sb₂Se₃ films should be improved irrespective of the deposition methods listed above [25, 28, 33–36, 44–46, 53–55, 69, 76, 78–85], while controlling the preferred crystal growth along the orientations [hk1]. In addition, the most promising technologies reported in [36, 46, 55, 78–85] may require serious improvements in the precursor systems and/or reaction yield, which make them later scalable to the industrial level.

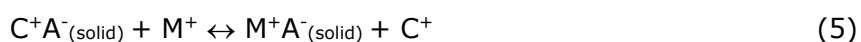
Summing up, since the typical deposition methods listed above suffer from a limited ability to eliminate secondary phases and control the orientation of [hk1] during the formation of Sb_2Se_3 thin films, a lot of additional effort is required using unusual approaches. In general, employing significant amounts of selenium source(s) in chemical methods such as CSP or CBD can partially suppress detrimental hydrolysis reactions, decreasing oxygen content in resulting materials. However, high prices of selenium-containing precursors (e.g. 618 EUR for 10g of selenourea [91]) and their low chemical stabilities practically prevents industrial applicability of such approaches. Thus, alternative synthetic ways to fabricate high-quality selenium-based layers, particularly antimony (III) selenide thin-film materials with their limited chemical stability, are much needed and may open new strategies to improve device performance.

1.4. Cation exchange

Cation exchange is a relatively old approach to transforming one compound into another, endowing the synthesised material with very specific or new properties [92]. Research activities carried out over the past three decades have demonstrated notable progress in the synthesis of various nano-scaled materials [93, 94], with minimal success reported for thin film materials.

1.4.1. Formation of cation exchanged materials

Cation exchange is characterised by a cation replacement in the crystal lattice [92]. Reactions of cation exchange occur in solid substances containing cations to be replaced and can be expressed using equation 5 [95]:



In which C^+A^- is a starting compound immersed into solution containing M^+ cations, M^+A^- is a formed new product. Cation exchange can be isovalent (equation 5) or non-isovalent (e.g. replacement of Cd(II) by Cu(I)) [95, 96]. In general, the cation replacement is realised via the following simplified steps (equations 6-9) [95]:

- Dissociation: $C^+A^- \leftrightarrow C^+ + A^-$ (6)
- Desolvation: $M^+(\text{sol}) \leftrightarrow M^+ + \text{sol}$ (7)
- Association: $M^+ + A^- \leftrightarrow MA$ (8)
- Solvation: $C^+ + \text{sol} \leftrightarrow C^+(\text{sol})$ (9)

Ion exchange can be controlled by both thermodynamic and kinetic factors [95]. Thermodynamics consist of crystal lattice energy, interfacial strain energy, dislocation energy, energy of dissociation and solvation; and cation exchange can be realised if [95]:

- a) Good solid-state mobility of both cations.
- b) Both cations are soluble in solvent, while the solubility of C^+ exceeds the solubility of M^+ ions.
- c) Product has lower total energy than a starting compound.
- d) Starting compound and product have crystal lattice constants enabling low strain anionic sublattice.
- e) Reaction occurs on a smaller area than crystal.

Kinetics determines the reaction rate and factors influencing it and controls the direction of reversible reactions. The result of cation exchange is mainly determined by the activation energy of each sub-reaction, and cation exchange can be facilitated by [95]:

- a) Temperature
- b) High surface area

Cation exchange is accelerated with increasing both temperature and ratio of surface area to volume [95]. There are many examples of various cation exchange reactions in nanocrystals [93, 94, 96–100] and only a few reports in bulk materials [101]. The nucleation energy barrier and activation energy are reduced in nanocrystals due to the huge surface area of a crystal with many defective states [95]. The reduced activation energy contributes to the formation of metastable phases via sub-reactions [95]. The nanocrystalline scale allows cation exchange to occur even at room temperature, since cations have higher access to the activated reactive centres [96].

As stated above, cation exchange could offer numerous protocols for synthesizing different nano-scaled metal selenide materials such as Cu_xSe , Ag_2Se , CdSe , ZnSe , PbSe , etc. [94, 102–105]. In general, the formation of metal chalcogenides is hindered when the value of Gibbs free energy is positive at elevated temperatures. In such conditions, non-spontaneous reactions to synthesize the desired products can be realised via a two-step process: a) transformation of starting compounds into intermediate copper or silver-based materials; b) fabricating the desired compounds by cation exchange in solutions containing target cations [94–96]. Controlling solution composition to minimize binding energy between solution components and target cations has been reported to increase the yield of cation exchange reactions occurred in nanocrystals [93, 94, 96–100]. Only a few reports found in the literature on the development of metal sulphide/selenide thin films indicate the complexity of the cation exchange approach to fabricating materials attached to the substrate.

1.5. Summary and aim of thesis

Antimony (III) selenide can be used for different applications and introduced as an absorber material in solar cell structures due to its direct bandgap of ~ 1.2 eV and a high absorption coefficient of 10^5 cm^{-1} [25].

Thin films of Sb_2Se_3 can be deposited using different physical or chemical deposition techniques. Irrespective of the physical methods used for depositing Sb_2Se_3 thin films, the formation of single-phase materials is complicated by partial decomposition at temperatures above 400°C [25, 28, 45, 54]. Chemical methods such as CSP and CBD have several advantages important for industrial implementation, including simple deposition setups and an ability to synthesize thin films rapidly over large-area substrates. ALD can offer deposition uniformity. Low reaction yield [72, 73] along with the chemical instability of selenium sources and their high prices may limit the industrial applicability of chemical approaches.

In physical and chemical methods, deposition temperature and precursor systems for antimony and selenium sources are the main parameters affecting the purity of the formed Sb_2Se_3 film and its crystallization along the undesired $[\text{hk}0]$ orientations. Regardless of the direct synthetic approaches, as-deposited Sb_2Se_3 thin films are contaminated by secondary phases or precursor-derived elements [33, 36, 53, 76]. Improving the properties of as-deposited Sb_2Se_3 films usually requires additional treatments, such as annealing to crystallize the amorphous content, selenization to approximate the composition to stoichiometric, and/or chemical treatment to reduce the oxygen content [80, 106–109]. Most traditional treatment procedures reported in the literature are still limited in eliminating secondary phases or sophisticated by fancy experimental setups to be applied [28, 36, 110].

Considering all the listed above, the indirect synthesis of Sb_2Se_3 using cation exchange applied to convert any available and stable metal selenide film is of great interest, since it could offer new routes to control the properties of formed films [92, 95]. No studies on the inversion of any metal selenide films into continuous Sb_2Se_3 thin films attached to the substrate have been reported in the literature.

Thus, the aim of the current thesis was to test the applicability of cation exchange to invert available SnSe thin films into continuous Sb_2Se_3 materials attached to the substrate.

2. EXPERIMENTAL PART

This part presents experimental details for the fabrication of thin films using Sn-to-Sb replacement in SnSe matrices and characterisation of formed materials.

2.1. Tin (II) Selenide deposition

SnSe thin films were deposited onto 10 cm x 10 cm substrates using magnetron sputtering (Evovac 030 inline coating system Angstrom Engineering, Kitchener, ON, Canada) under argon pressure of 1 mTorr. Substrate temperatures were varied from RT to 300 °C. The target was commercially available tin (II) selenide (LOT: PLA546838312, Plas-materials, Inc., Livermore, CA, USA). The distance between the target and the substrate was kept at 20 cm. During sputtering, plasma power was 88 kW. The resulting film thickness was 700 nm. After deposition, the films were cooled to RT for 2 hours.

2.2. Sn-to-Sb replacement

Cation exchange was performed by immersing as-deposited SnSe thin films in glycerol solutions containing SbCl_3 in different concentrations. The samples were placed horizontally on the bottom of the bath, completely opening the surface of the film for the solution. Solutions were prepared by dissolving a proper amount of SbCl_3 (p.a. > 99%, Sigma-Aldrich, Darmstadt, Germany) in glycerol (LOT: 2058170, Fisher Scientific, Inc., Waltham, MA, USA). The concentration of SbCl_3 in glycerol solutions were varied from 11 to 44 mM. Cation exchange was carried out at ~ 210 °C. Reaction time ranged from 1 to 22 min.

After the cation exchange was completed, the reaction vessels were placed in an ice bath to terminate the process. Then the samples were washed with deionized water, dried with air, and thermally treated in an argon atmosphere at 400 °C for 15 minutes to ensure crystallinity.

2.3. Characterisation

All formed films were characterised using numerous techniques to reveal changes initiated by cation replacement.

Scanning Electron Microscopy with Energy Dispersive X-Ray Analysis

The surface morphologies, cross-sectional views, and elemental compositions of the obtained films were investigated using a Zeiss Merlin scanning electron microscope (Oerzen, Germany) equipped with the Bruker EDX-XFlash6/30 detector. The SEM and EDX measurements were performed at acceleration voltages of 3 kV and 20 kV, respectively.

SEM deploys a focused electron beam to obtain certain signals from the sample surface [111]. The signals are divided into secondary electrons, backscattered electrons, and characteristic X-rays. Secondary electrons are caused by inelastic electron-surface interactions and reveal the topography and morphology of the studied sample. Backscattered electrons resulted from elastic electron-surface interactions and provide details on the contrast of the sample phases. They are sensitive to the atomic number of the studied material. Characteristic X-rays exhibit elemental particulars of the sample [111].

XRD

Structural analysis of the samples was carried out using a Rigaku Ultima IV diffractometer (Neu-Isenburg, Germany) with monochromatic Cu K α 1 radiation ($\lambda = 1.5406 \text{ \AA}$) at 40 kV and 40 mA equipped with a D/teX Ultra silicon strip detector. X-ray diffractograms were collected in a 2θ range of 10-70° with a step of 0.02°.

X-ray diffraction occurs when an incident beam of X-rays interferes with uniformly spaced crystal atoms [112–114]. A beam of X-rays contacts crystal planes with an angle of incidence θ and is reflected from them at the same angle. X-rays are constructively scattered from the atomic planes that are an interplanar distance d apart according to the Bragg law:

$$n\lambda = 2d \sin\theta \quad (10)$$

where n is a diffraction order, λ the incident X-ray wavelength, d is the interplanar distance and θ is the Bragg angle.

The crystallite size (D) can be calculated using Scherrer's relation 11:

$$D = \frac{K\lambda}{\beta \cos\theta} \quad (11)$$

where λ is the wavelength of the X-ray radiation (1.5406 Å), θ is the Bragg angle, K is a geometrical constant (equal to 0.94), and β is the full width at the half-maximum (fwhm) of the given peak in radians. The lattice constants of Sb₂Se₃ can be defined using the following equation 12:

$$\frac{1}{d^2} = \frac{h^2}{a^2} + \frac{k^2}{b^2} + \frac{l^2}{c^2} \quad (12)$$

where (hkl) are the Miller indices, and d is the interplanar distance.

Raman spectroscopy

Raman spectroscopy was used to define the phase composition and chemical structure of the prepared thin films. The Raman spectra were measured on a Horiba LabRam HR800 spectrometer (Oberursel, Germany) in the Raman shift range of 50–600 cm⁻¹ using the green laser focused on a spot with a diameter of 100 μm.

Raman spectroscopy is based on the interaction of light with the materials' chemical bonds [115]. The incident light coming from the laser is mostly scattered by a molecule at the same wavelength as the laser (Rayleigh scatter), providing no useful data. Chemical structure of the examined material can be determined from a very small amount of light scattered at different wavelengths (Raman scatter). Raman spectra consist of numerous peaks positioned at different wavelengths that are correlating with vibrations of certain molecular bonds [115].

Ultraviolet-visible spectroscopy

The incident light interacts with the examined material resulting in light absorption, reflection, or transmission [116, 117]. Optical transmittance spectra of films were measured in the range of 300-2000 nm using a Cary 5000 UV-Vis-NIR spectrophotometer (Agilent Technologies, Inc., Santa Clara, CA, USA). The optical bandgap (E_g) values of films can be estimated using the Tauc equation 13 by extrapolating the straight-line portion of the $(\alpha h\nu)^2$ versus $h\nu$ graph to a zero-absorption coefficient value:

$$(\alpha \cdot h\nu)^n = A(h\nu - E_g) \quad (13)$$

where α is the absorption coefficient, h is the Planck constant, A is the constant, which is independent from the photon energy, E_g is a bandgap energy, $h\nu$ is the incident photon energy, and $n=2$ for the direct transitions [118–120].

3. RESULTS AND DISCUSSION

3.1. Preliminary experiments

Despite the negative values of Gibbs free energy in the temperature range of 20-400 °C, the formation of Sb_2Se_3 according to the reaction 14 meets many technical problems:



Several attempts have been tested to find suitable conditions to keep the formed materials on substrates.

Solvent

Solutions based on methanol, propanol and acetone were unable to initiate a noticeable cation exchange regardless of the treatment temperature and used concentrations of SbCl_3 . Thus, glycerol was used as a solvent due to its ability to operate in much wider temperature window.

Templating SnSe

Templating SnSe matrices at temperatures below 250 °C accelerated peeling off the films from the typical substrates such as soda-lime glass, Mo, FTO, ITO, even if pure glycerol was used. Only depositions at temperatures exceeding 250-300 °C allow SnSe matrices to remain on Mo, FTO, and ITO substrates.

Approaching the correct SbCl_3 concentrations

Inversion of SnSe into Sb_2Se_3 occurred when pristine films grown at 300 °C were treated with SbCl_3 solutions at concentrations of 90, 135, 180 mM (Figure 8). Even the lowest tested concentration of 90 mM destroyed the adhesion between the formed material and the substrate, indicating the need to further reduce the concentration of SbCl_3 in solution.

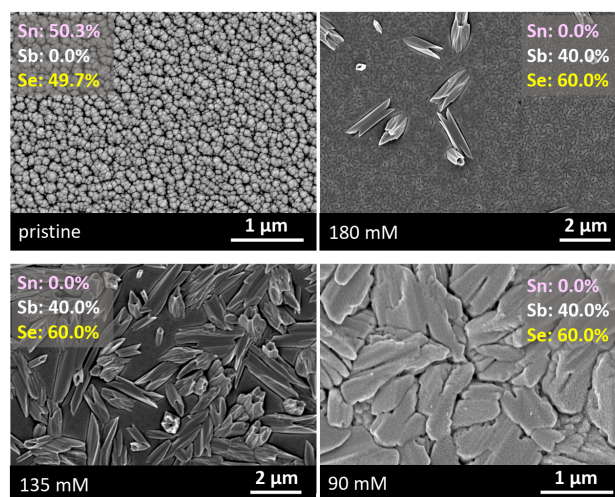


Figure 8. Top-view images of the samples treated for 25 min using solutions containing different amounts of SbCl_3 in glycerol. EDX data collected from the parts of treated materials remaining on Mo substrates.

3.2. Effect of reducing SbCl_3 concentration

Morphology and elemental composition

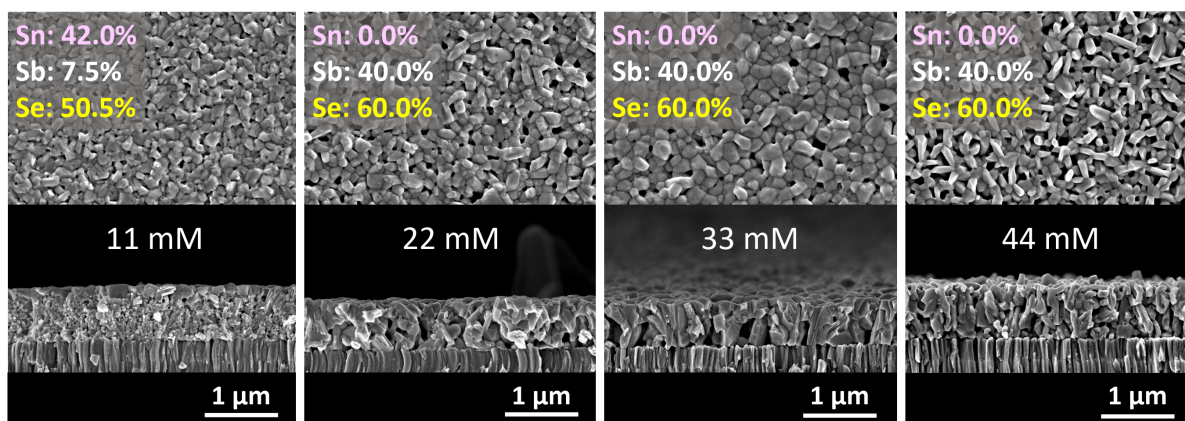


Figure 9. Top-view and cross-sectional images of the samples treated for 22 min with various concentration.

A further decrease in SbCl_3 concentrations (below 45 mM) stabilized exchange processes in the materials attached to the substrate. After overcoming several of the above limitations, the materials undergoing cation exchange treatments show compact and continuous structural characteristics, an entire thickness of about 700 nm, and relatively good adhesion, allowing post-treatment washing, drying and further use. The formation of a pin-hole free layer indicates that corrosion processes were minimized during cation exchange (Figure 9). The thickness of the formed layers is similar to the value measured for the original SnSe thin-film material. This fact confirms the main aspect of cation

exchange, postulating that anions are not substituted in a cation exchange reaction (Figure 9).

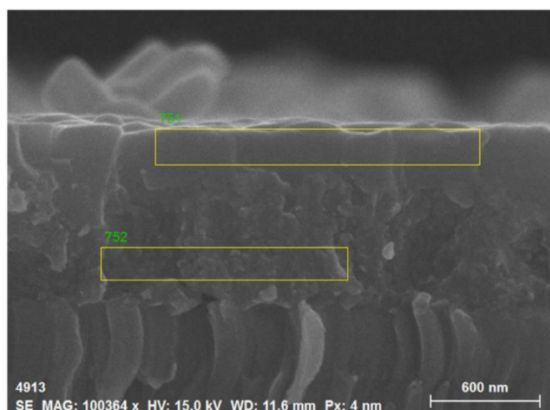


Figure 10. Magnified cross-sectional image of the sample experienced treatment in 11 mM SbCl_3 solution for 22 min.

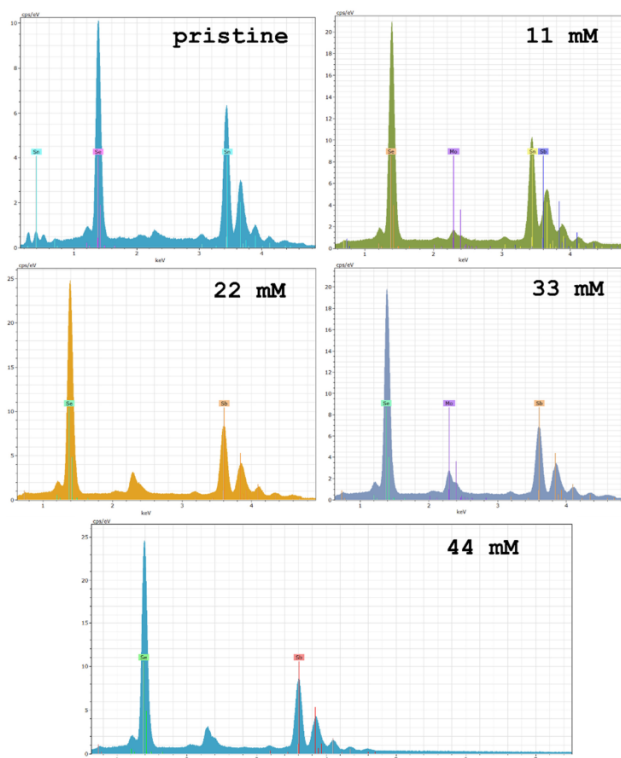


Figure 11. EDX spectra of the pristine SnSe film and those treated in glycerol at various concentrations of SbCl_3 for 22 min.

Close examination of the sample treated in 11 mM SbCl_3 solution revealed the formation two-layered structure (Figure 9). According to EDX data, the top layer (751) contained 35.5 at.% Sn, 13.8 at.% Sb and 50.6 at.% Se, whereas the bottom layer consisted of 46.0 at.% Sn, 3.9 at.% Sb and 50.2 at.% Se. EDX analysis confirmed the complete transformation of the films treated using 22, 33 and 44 mM solutions, as only signals from Sb and Se were recorded at atomic ratios of $\sim 2:3$ (Figures 9, 11).

Structural analysis

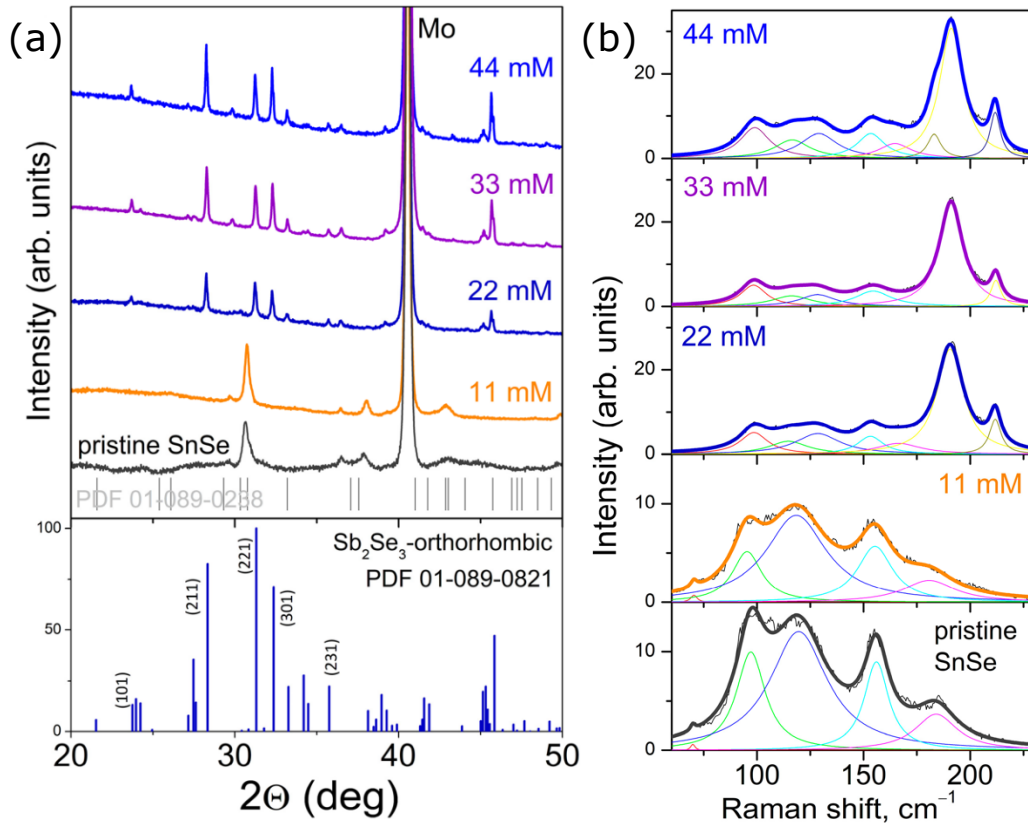


Figure 12. (a) XRD patterns and (b) Raman spectra of the samples treated for 22 min in solutions with different amounts of SbCl₃.

Structural characteristics of the films experienced cation exchange treatments were investigated using X-ray diffraction and Raman spectroscopy (Figure 12). After the complete transformation according to EDX analysis, XRD patterns of the 22, 33, and 44 mM-treated samples show peaks that are well consistent with the reflections of the orthorhombic Sb₂Se₃ phase in PDF card No.: 01-089-0821 (Figure 10). Furthermore, all the formed Sb₂Se₃ layers crystallize along (101), (211), (221), (301), (311), and (151) planes, which correspond to vertically aligned (Sb₄Se₆)_n ribbons [42] that are necessary for adequate transporting charge carriers in the absorber layer.

The Raman spectrum of the pristine SnSe reveals five obvious peaks centred at around 70, 97, 120, 156, and 184 cm⁻¹ (black curve in Figure 12b) [121], which differ from those at around 99, 116, 129, 153, 191, and 212 cm⁻¹ (royal blue curve in Figure 12b, 22 mM sample), typical Raman characteristics for Sb₂Se₃ [122, 123]. Thus, Raman measurements confirm the data derived from both XRD and EDX studies that concentrations of SbCl₃ exceeding 11 mM induce the complete transition of SnSe templates to Sb₂Se₃.

3.3. Effect of time treatment

Morphology and elemental composition

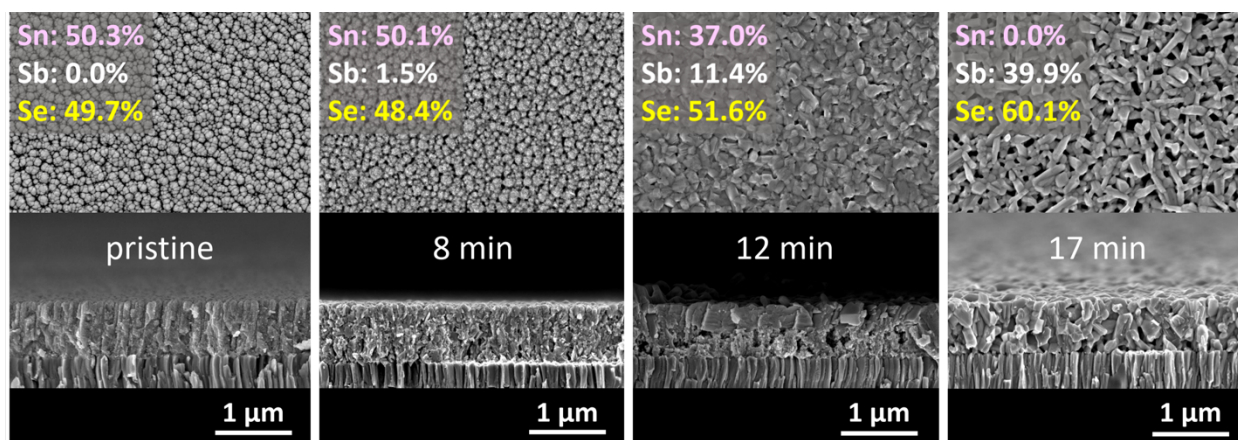


Figure 13. SEM images and EDX data of the layers experienced cation exchange in 44 mM SbCl₃ solutions for a different time.

Table 3. Atomic percentages of tin, antimony, and selenium according to the EDX data developed in 44 mM SbCl₃ solutions within different time treatments.

Treatment	Time (min)	Elements (at.%)		
		Sn	Se	Sb
pristine	bare	51.0	49.0	-
44 mM SbCl ₃	5	51.0	49.0	-
	6	51.0	49.0	-
	7	50.2	48.5	1.3
	8	50.1	48.4	1.5
	9	43.5	49.9	6.6
	10	42.7	49.4	7.9
	12	37.0	51.6	11.4
	17	-	60.1	39.9
	22	-	60.0	40.0

Noticeable Sn-to-Sb substitution starts after treatment lasting for 7 min. A longer process of 10 min increases the content of Sb up to 7.9 % (Table 3), with higher Sb concentrations on the film surface and lower concentrations close to the Mo-substrate, similarly to those shown in Figure 10. Cation exchange during 12 min leads to further accumulation of Sb in the layer up to ~ 11.4 %, reaching critical conditions for a notable phase transition (Table 4). Processing during 17 and 22 min yields to complete elimination of Sn contents from the samples (Table 3).

Structural analysis

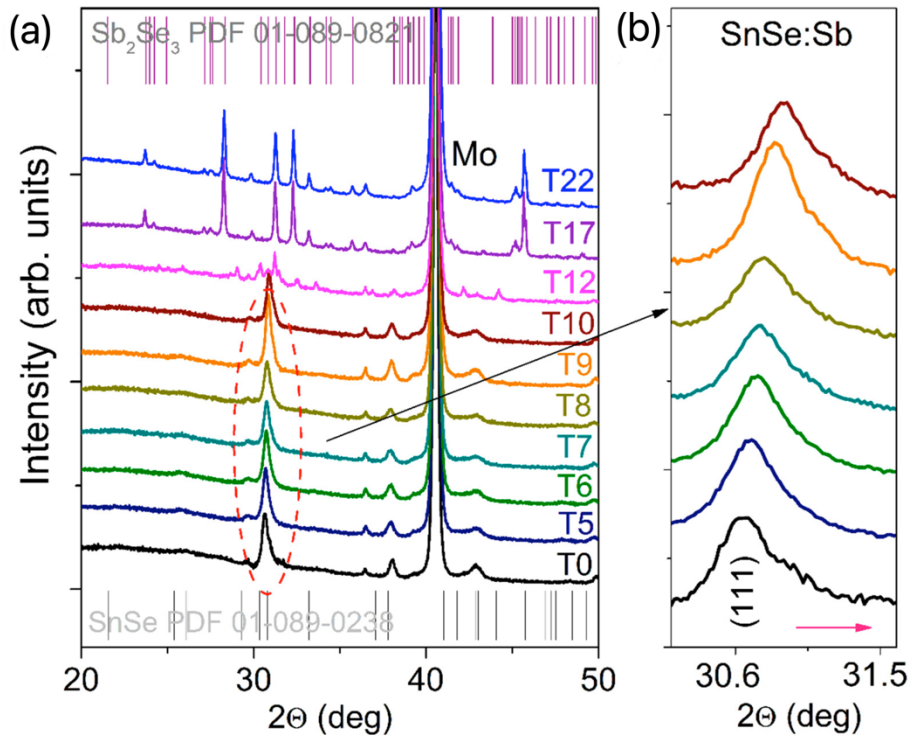


Figure 14. (a) XRD patterns of films treated in 44 mM SbCl_3 solution for a different time. (b) Magnified XRD patterns of the (111) peak of the pristine SnSe and antimony-doped SnSe layers.

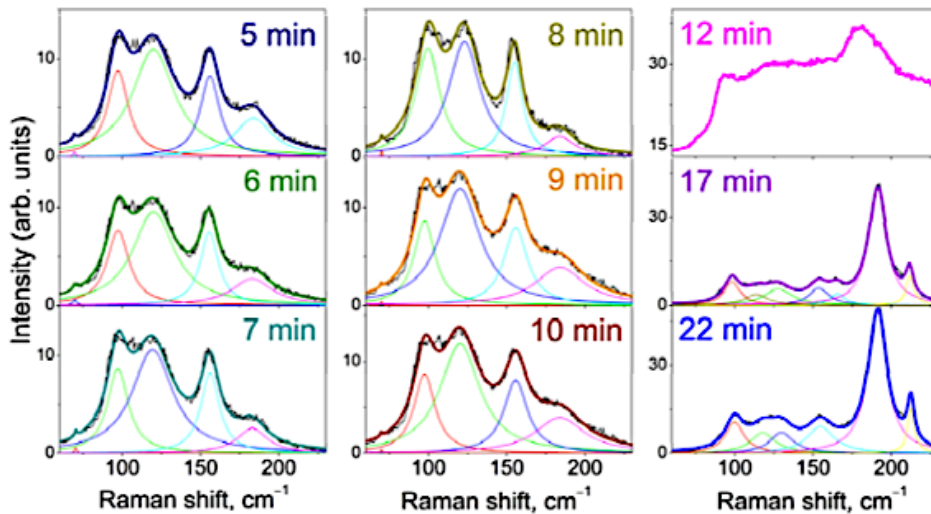


Figure 15. Raman spectra of films treated in 44 mM SbCl_3 solution for a different time.

The initial treatment in the 44 mM SbCl_3 solution for 5 min shows minimal effect on the elemental (Table 3) and phase compositions of the sample (Figures 14), however it significantly increases the crystallite size of the SnSe phase and changes its lattice parameters to the bulk values (Table 4). This fact indicates the absence of internal stress

due to incorporating Sn ions. A slightly longer processing from 6 to 9 min provokes a decrease in the lattice parameters along with the a and b axes, as confirmed by a notable shift of the (111) XRD peak towards higher 2θ values (Figure 14), and a shift in Raman peak positions to lower wavenumbers (Figure 15). Such behavior might be associated with the formation of tin vacancies.

Table 4. Main phase according to XRD and Raman, the average crystallite size (D), and lattice parameters developed in 44 mM SbCl_3 solutions within different time treatments. Each parameter was determined by averaging the values obtained from three measurements for each sample. The error represents the standard deviation.

Treatment	Time (min)	Main phase	D (nm) (± 1)	Lattice parameters (\AA) (± 0.001)		
				a	b	c
pristine	bare	SnSe	20	11.670	4.201	4.353
44 mM SbCl_3	5	SnSe	40	11.611	4.216	4.397
	6	SnSe	25	11.572	4.206	3.383
	7	SnSe	22	11.534	4.204	4.440
	8	SnSe	21	11.505	4.202	4.343
	9	SnSe	20	11.441	4.185	4.403
	10	SnSe	19	11.420	4.163	4.441
	12	Sn_3SbSe_4				
	17	Sb_2Se_3	79	11.611	11.737	3.970
22	Sb_2Se_3	97	11.611	11.719	3.970	
SnSe PDF Card No.: 01-089-0238				11.611	4.216	4.397

As stated above, the 12 min process promotes the inclusion of significant amounts of Sb in the film (Table 3), creating conditions for a phase transition. Several XRD peaks located at 25.9° , 29.0° , 30.3° , and 44.1° (Figure 14) deviate from those observed in the XRD patterns of synthesized SnSe and Sb_2Se_3 films, hinting at an intermediate crystal structure. Raman studies support the data obtained from XRD and SEM/EDX measurements on evolution of a ternary compound from a family of $\text{Sn}_x\text{Sb}_y\text{Se}_z$, revealing the bands that differ from those of SnSe and Sb_2Se_3 (Figure 15). The XRD patterns and Raman spectra of the 17 and 22 min processed samples are completely different from the ground state and the 12-min exposed sample, showing the reflections of Sb_2Se_3 phase only (Figures 14, 15). According to XRD, a significant increase in crystallite size is observed after the transformation of SnSe matrix into Sb_2Se_3 (Table 4).

Optical studies

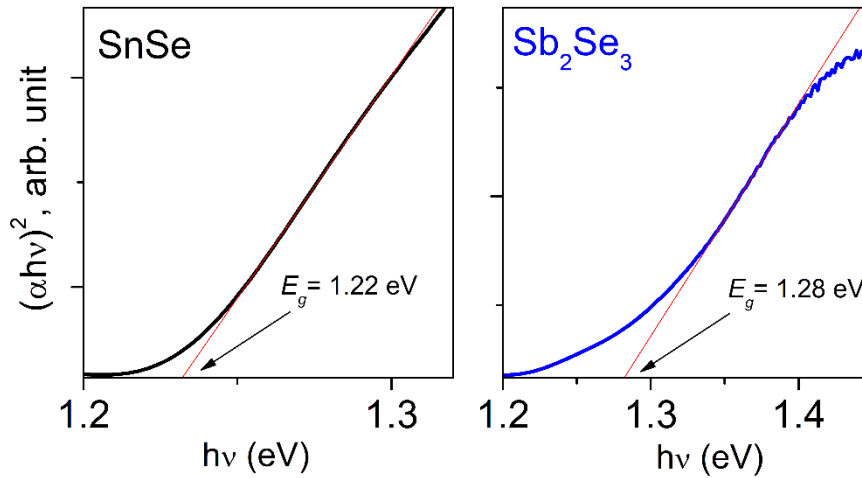


Figure 16. Tauc plots of the pristine SnSe film and that Sb_2Se_3 sample being treated in 44 mM $SbCl_3$ solution for 22 min. Direct bandgaps were calculated by extrapolating the straight-line portion of the $(\alpha h\nu)^2$ versus $h\nu$ graph to a zero-absorption coefficient.

The optical bandgap values of the ground SnSe state and the sample being inverted into Sb_2Se_3 were determined from the optical transmission data using the Tauc relation (Figure 16). The optical transmittance spectra were collected for the samples attached to FTO substrates. According to UV-Vis, the pristine SnSe film exhibited a bandgap value of 1.22 eV [124]. The bandgap of Sb_2Se_3 films being inverted in the 44 mM $SbCl_3$ solution for 22 min display a bandgap of 1.28 eV, typical characteristic of the orthorhombic Sb_2Se_3 phase [28]. Thus, the optical data matches the data from EDX, XRD, and Raman measurements.

4. CONCLUSIONS

This work aimed at testing the applicability of cation exchange synthetic routes to transform tin (II) selenide thin films into continuous antimony (III) containing selenide materials attached to the rigid substrates. Antimony (III) selenide as a result of complete Sn-to-Sb inversion is a perspective absorber for photovoltaic applications. Numerous studies have reported the transformations of separately standing nano-objects with almost no success demonstrated for inverting thin films materials. To date, the formation of Sb_2Se_3 thin films by cation exchange has not been reported. Effective cation replacement realized in extended solids could open a new way to synthesize high-quality optoelectronic materials developed on the scale of attached-to-substrate thin films.

To conclude, the main outcomes of this work can be formulated as follows:

1. Cation exchange performed can be applied to form Sb-containing selenide materials attached to the substrates when sputtered SnSe thin films are used as matrices.
2. Time treatment, concentrations of SbCl_3 in glycerol, and substrate type were found to be critical parameters to control cation exchange processes realized on the FTO, ITO, Mo substrates.
3. Templating the SnSe matrices by magnetron sputtering at temperatures below $250\text{ }^\circ\text{C}$ yielded to poor adhesion between the formed materials and substrate irrespective of used the substrate type, time treatment and SbCl_3 concentrations. Films remained on the substrates when SnSe films were sputtered at substrate temperatures of at least $300\text{ }^\circ\text{C}$.
4. Concentrations of SbCl_3 in glycerol between 11 and 45 mM and time treatments exceeding 5 min initiated cation exchange in SnSe films at converting temperatures of about $210\text{ }^\circ\text{C}$. Concentrations of Sb gradually increased in the formed layers by increasing both SbCl_3 molarity to 45 mM and processing time to 12 min.
5. Concentration of SbCl_3 close to 45 mM and treatment lasting for 12 min generated the conditions for forming an intermediate crystal structure, supposedly Sn_3SbSe_4 .
6. Increasing further the processing time to 17 and 22 min in 44 mM SbCl_3 solutions led to a complete SnSe-to- Sb_2Se_3 transformation. The inverted Sb_2Se_3 films were

stoichiometric, consisted of the orthorhombic Sb_2Se_3 phase crystallized along (hk1) planes with a crystallite size of about 80 nm, and exhibited an optical bandgap value of 1.28 eV.

SUMMARY

Solar energy is an alternative renewable source of energy, and, with its help, the humanity may fully transit to renewable energy sources and overcome energy. Photovoltaics are available semiconductor materials to use and maintain. Late research are focused on increasing efficiency of solar cells and finding alternatives to existing toxic and scarce materials. Therefore, one of the promising substitutes to those could be antimony (III) selenide.

Antimony (III) selenide has properties suitable for an absorber layer in PV application such as a close-to-ideal optical band gap, high absorption coefficient as well as earth crust abundance and non-toxicity of the compound. Sb_2Se_3 absorber layer can be fabricated using various industrial deposition techniques. However, different difficulties during deposition affect the resulting Sb_2Se_3 thin film properties. As an alternative method to the current industrial deposition techniques, ion exchange can be introduced. The technique could offer such advantages as simplicity, cost- and yield-effectiveness.

In this work, SnSe thin films acted as matrices in the cation exchange process and were magnetron-sputtered onto various substrates at different temperatures. The cation exchange process was performed at 210 °C in the SbCl_3 solutions of different solvents, concentrations and time treatments. Glycerol was chosen as the most suitable solvent for the treatment.

It was concluded that substrate type, SbCl_3 solution molarity and time treatment were the critical parameters for the cation exchange process. SnSe thin films deposited onto a glass substrate peeled off regardless SbCl_3 solution concentrations and time treatment applied. SnSe films deposited at temperatures above 300 °C onto Mo, FTO, ITO withstood cation exchange at concentrations below 45 mM. Time treatment ranged from 1 to 22 min.

SbCl_3 solution concentrations between 11 and 45 mM initiated the SnSe-to- Sb_2Se_3 full transformation. Time treatments exceeding 5 min induced the SnSe-to- Sb_2Se_3 conversion. Further time treatment raise increased Sb content in the films. Time treatments of 17 and 22 min in 44 mM solution led to the full inversion of SnSe thin films into Sb_2Se_3 . Formed Sb_2Se_3 thin films consisted of orthorhombic Sb_2Se_3 crystals oriented along (hk1) planes, exhibited stoichiometric Sb/Se atomic ratio and a direct optical band gap of 1.28 eV.

LIST OF REFERENCES

- [1] International Energy Agency, "Statistics report Key World Energy Statistics 2021," 2021. Accessed: Jan. 04, 2023. [Online]. Available: <https://www.iea.org/reports/key-world-energy-statistics-2021/supply>
- [2] Grantham Research Institute on Climate Change and the Environment, "Climate Change Laws of the World." <https://climate-laws.org> (accessed Jan. 04, 2023).
- [3] J. Pastuszak and P. Węgierek, "Photovoltaic Cell Generations and Current Research Directions for Their Development," *Materials*, vol. 15, no. 16. MDPI, Aug. 01, 2022. doi: 10.3390/ma15165542.
- [4] A. Zakutayev, "Brief review of emerging photovoltaic absorbers," *Current Opinion in Green and Sustainable Chemistry*, vol. 4. Elsevier B.V., pp. 8–15, Apr. 01, 2017. doi: 10.1016/j.cogsc.2017.01.002.
- [5] K. Zeng, D. J. Xue, and J. Tang, "Antimony selenide thin-film solar cells," *Semiconductor Science and Technology*, vol. 31, no. 6. Institute of Physics Publishing, Apr. 19, 2016. doi: 10.1088/0268-1242/31/6/063001.
- [6] D. R. Lide, *CRC Handbook of Chemistry and Physics*, 84th ed. 2003.
- [7] J. D. (John D. Smith, *The chemistry of arsenic, antimony and bismuth*, 1st ed. Pergamon Press, 1975.
- [8] Mamta, Y. Singh, K. K. Maurya, and V. N. Singh, "A review on properties, applications, and deposition techniques of antimony selenide," *Solar Energy Materials and Solar Cells*, vol. 230. Elsevier B.V., Sep. 15, 2021. doi: 10.1016/j.solmat.2021.111223.
- [9] G. Ghosh, "The Sb-Se (Antimony-Selenium) System," *Journal of Phase Equilibria*, vol. 14, no. 6, pp. 753–763, 1993.
- [10] G. Gospodinov, B. Popovkin, A. Pashinkin, and A. V. Novoselova, "Investigation of Bismuth Sulfide, Antimony Sulfide and Antimony Selenide Behavior Under Sublimation," *Vestn. MosL Univ., Khim*, vol. 22, no. 2, pp. 54–57, 1967.
- [11] V. Ban and B. Knox, "Mass-Spectrometric Study of Laser-Induced Vaporization of Compounds of Arsenic and Antimony with the Elements of Group VIB," *J. Chem Phys.*, pp. 248–253, 1970.
- [12] B. Predel, E. Gerdes, and U. Gerling, "Influence of Associates in the VaporPhase on Activity Determination and the Revision of Activities of Selenium-Thallium, Selenium-Bismuth and Selenium-Antimony Liquid Alloys, in German.," *Z. Metallkd.*, pp. 109–112, 1979.
- [13] A. Hoareau, B. Cabaud, and R. Uzan, "Mass Spectrometry: Study of SbSe Type of Compositions by Mass Spectrometry, in French," *C. R. Acad. Sci. Paris*, pp. 705–707, 1972.
- [14] W. Gierlotka, I. tsen Lin, S. wen Chen, W. Gaşior, and A. Dębski, "Re-optimization of the binary Sb – Se system aided by ab-initio calculations," *CALPHAD*, vol. 73, Jun. 2021, doi: 10.1016/j.calphad.2021.102257.

- [15] N. W. Tideswell, F. H. Kruse, and J. D. McCullough, "The Crystal Structure of Antimony Selenide, Sb_2Se_3 ," *Acta Cryst.*, vol. 10, no. 99, pp. 99–102, 1957.
- [16] A. Mavlonov *et al.*, "A review of Sb_2Se_3 photovoltaic absorber materials and thin-film solar cells," *Solar Energy*, vol. 201. Elsevier Ltd, pp. 227–246, May 01, 2020. doi: 10.1016/j.solener.2020.03.009.
- [17] B. Bauerhenne, E. S. Zijlstra, and M. E. Garcia, "Molecular dynamics simulations of a femtosecond-laser-induced solid-to-solid transition in antimony," *Appl Phys A Mater Sci Process*, vol. 123, no. 9, Sep. 2017, doi: 10.1007/s00339-017-1216-7.
- [18] P. Cherin and P. Unger, "The Crystal Structure of Trigonal Selenium," *Adv Chem Ser*, vol. 6, no. 8, pp. 1589–1591, 1967, [Online]. Available: <https://pubs.acs.org/sharingguidelines>
- [19] S. Imura, T. Watabe, K. Miyakawa, K. Hagiwara, H. Ohtake, and M. Kubota, "Effects of grain refinement on surface enhancement of thin-film chlorine-doped crystalline selenium," *Journal of Materials Science: Materials in Electronics*, vol. 28, no. 10, pp. 7064–7069, May 2017, doi: 10.1007/s10854-016-6311-6.
- [20] C. Svensson, "Refinement of the Crystal Structure of Cubic Antimony Trioxide, Sb_2O_3 ," *Acta Cryst*, vol. 31, 2016.
- [21] "The Materials Project." <https://materialsproject.org/> (accessed Nov. 08, 2022).
- [22] D. Orosel, P. Balog, H. Liu, J. Qian, and M. Jansen, " Sb_2O_4 at high pressures and high temperatures," *J Solid State Chem*, vol. 178, no. 9, pp. 2602–2607, Sep. 2005, doi: 10.1016/j.jssc.2005.05.037.
- [23] L. Zhang *et al.*, "Scalable Low-Band-Gap Sb_2Se_3 Thin-Film Photocathodes for Efficient Visible-Near-Infrared Solar Hydrogen Evolution," *ACS Nano*, vol. 11, no. 12, pp. 12753–12763, Dec. 2017, doi: 10.1021/acsnano.7b07512.
- [24] C. Chen *et al.*, "Characterization of basic physical properties of Sb_2Se_3 and its relevance for photovoltaics," *Frontiers of Optoelectronics*, vol. 10, no. 1, pp. 18–30, Mar. 2017, doi: 10.1007/s12200-017-0702-z.
- [25] C. Chen *et al.*, "Optical properties of amorphous and polycrystalline Sb_2Se_3 thin films prepared by thermal evaporation," *Appl Phys Lett*, vol. 107, no. 4, Jul. 2015, doi: 10.1063/1.4927741.
- [26] T. D. C. Hobson *et al.*, "P-type conductivity in Sn-doped Sb_2Se_3 ," *Journal of Physics: Energy*, vol. 4, no. 4, p. 045006, Oct. 2022, doi: 10.1088/2515-7655/ac91a6.
- [27] T. D. C. Hobson *et al.*, "Isotype Heterojunction Solar Cells Using n-Type Sb_2Se_3 Thin Films," *Chemistry of Materials*, vol. 32, no. 6, pp. 2621–2630, Mar. 2020, doi: 10.1021/acs.chemmater.0c00223.
- [28] X. Liu *et al.*, "Thermal evaporation and characterization of Sb_2Se_3 thin film for substrate Sb_2Se_3/CdS solar cells," *ACS Appl Mater Interfaces*, vol. 6, no. 13, pp. 10687–10695, Jul. 2014, doi: 10.1021/am502427s.
- [29] D. B. Li *et al.*, "Stable and efficient CdS/Sb_2Se_3 solar cells prepared by scalable close space sublimation," *Nano Energy*, vol. 49, pp. 346–353, Jul. 2018, doi: 10.1016/j.nanoen.2018.04.044.

- [30] L. J. Phillips *et al.*, "Close-Spaced Sublimation for Sb₂Se₃ Solar Cells Co-sputtered MgZnO window layers for CdTeSe solar cells View project Geopop View project Close-Spaced Sublimation for Sb₂Se₃ Solar Cells," 2018. [Online]. Available: <https://www.researchgate.net/publication/318495290>
- [31] X. Liang *et al.*, "Effect of deposition pressure on the properties of magnetron sputtering-deposited Sb₂Se₃ thin-film solar cells," *Appl Phys A Mater Sci Process*, vol. 125, no. 6, Jun. 2019, doi: 10.1007/s00339-019-2677-7.
- [32] R. Tang *et al.*, "Controlled sputtering pressure on high-quality Sb₂Se₃ thin film for substrate configured solar cells," *Nanomaterials*, vol. 10, no. 3, Mar. 2020, doi: 10.3390/nano10030574.
- [33] N. Mahuli, D. Halder, A. Paul, and S. K. Sarkar, "Atomic Layer Deposition of an Sb₂Se₃ Photoabsorber Layer Using Selenium Dimethyldithiocarbamate as a New Se Precursor," *Chemistry of Materials*, vol. 31, no. 18, pp. 7434–7442, Sep. 2019, doi: 10.1021/acs.chemmater.9b02085.
- [34] K. Y. Rajpure and C. H. Bhosale, "Effect of Se source on properties of spray deposited Sb₂Se₃ thin films."
- [35] K. Y. Rajpure and C. H. Bhosale, "Preparation and characterization of spray deposited photoactive Sb₂S₃ and Sb₂Se₃ thin films using aqueous and non-aqueous media," 2002.
- [36] Y. Zhao *et al.*, "Regulating deposition kinetics via a novel additive-assisted chemical bath deposition technology enables fabrication of 10.57%-efficiency Sb₂Se₃ solar cells," *Energy Environ Sci*, 2022, doi: 10.1039/D2EE02261C.
- [37] L. Holland, F. P. Inst, P. S. Tolansky, and J. Wiley, "Vacuum Deposition of Thin Films," 1958.
- [38] J. Orava, T. Kohoutek, and T. Wagner, "Deposition techniques for chalcogenide thin films," in *Chalcogenide Glasses*, Elsevier Ltd., 2013, pp. 265–309. doi: 10.1533/9780857093561.1.265.
- [39] H. Soonmin, "Thermal Evaporation of Thin Films: Review," *Middle-East Journal of Scientific Research*, vol. 23, no. 11, pp. 2695–2699, 2015, doi: 10.5829/idosi.mejsr.2015.23.11.22638.
- [40] O. Åke, B. Noläng, E. G. Osadchii, L.-O. Öhman, and E. Rosén, "Chemical Thermodynamics Of Selenium," *OECD Nuclear Energy Agency, Data Bank*. OECD Nuclear Energy Agency, 2004.
- [41] G. Gospodinov, A. Pashinkin, Z. Boncheva-Mladenova, and A. Novoselova, "Determination of the Saturated Vapour Pressure of Solid Antimony Selenide," *Fiz. Mater.*, vol. 6, p. 726, 1970.
- [42] Y. Zhou *et al.*, "Thin-film Sb₂Se₃ photovoltaics with oriented one-dimensional ribbons and benign grain boundaries," *Nat Photonics*, vol. 9, no. 6, pp. 409–415, Jun. 2015, doi: 10.1038/nphoton.2015.78.
- [43] N. Amin and K. S. Rahman, "Close-Spaced Sublimation (CSS): A Low-Cost, High-Yield Deposition System for Cadmium Telluride (CdTe) Thin Film Solar Cells," in *Modern Technologies for Creating the Thin-film Systems and Coatings*, InTech, 2017, pp. 362–379. doi: 10.5772/66040.

- [44] L. J. Phillips *et al.*, "Close-Spaced Sublimation for Sb₂Se₃ Solar Cells," in *IEEE PVSC 44*, 2017.
- [45] O. S. Hutter, L. J. Phillips, K. Durose, and J. D. Major, "6.6% efficient antimony selenide solar cells using grain structure control and an organic contact layer," *Solar Energy Materials and Solar Cells*, vol. 188, pp. 177–181, Dec. 2018, doi: 10.1016/j.solmat.2018.09.004.
- [46] N. Spalatu *et al.*, "Screening and optimization of processing temperature for Sb₂Se₃ thin film growth protocol: Interrelation between grain structure, interface intermixing and solar cell performance," *Solar Energy Materials and Solar Cells*, vol. 225, Jun. 2021, doi: 10.1016/j.solmat.2021.111045.
- [47] F. Shi, "Provisional chapter Introductory Chapter: Basic Theory of Magnetron Sputtering 1. Principle of magnetron sputtering," 2016.
- [48] I. V. Tudose *et al.*, "Chemical and physical methods for multifunctional nanostructured interface fabrication," in *Functional Nanostructured Interfaces for Environmental and Biomedical Applications*, Elsevier, 2019, pp. 15–26. doi: 10.1016/B978-0-12-814401-5.00002-5.
- [49] Angstrom Engineering, "Magnetron Sputtering: Overview." <https://angstromengineering.com/tech/magnetron-sputtering/> (accessed Oct. 28, 2022).
- [50] Angstrom Engineering, "DC Sputtering." <https://angstromengineering.com/tech/magnetron-sputtering/dc-sputtering/> (accessed Oct. 28, 2022).
- [51] Angstrom Engineering, "RF Sputtering." <https://angstromengineering.com/tech/magnetron-sputtering/rf-sputtering/> (accessed Oct. 28, 2022).
- [52] C. Charpentier, "Investigation of deposition conditions and annealing treatments on sputtered ZnO:Al thin films: Material properties and application to microcrystalline silicon solar cells," Ecole Polytechnique, 2013. [Online]. Available: <https://pastel.archives-ouvertes.fr/pastel-00801746>
- [53] G. Spaggiari *et al.*, "Growth and structural characterization of Sb₂Se₃ solar cells with vertical Sb₄Se₆ ribbon alignment by RF magnetron sputtering," *J Phys D Appl Phys*, vol. 54, no. 38, Sep. 2021, doi: 10.1088/1361-6463/ac0eb5.
- [54] G. X. Liang *et al.*, "Thermally induced structural evolution and performance of Sb₂Se₃ films and nanorods prepared by an easy sputtering method," *Solar Energy Materials and Solar Cells*, vol. 174, pp. 263–270, Jan. 2018, doi: 10.1016/j.solmat.2017.09.008.
- [55] R. Tang *et al.*, "Highly efficient and stable planar heterojunction solar cell based on sputtered and post-selenized Sb₂Se₃ thin film," *Nano Energy*, vol. 64, Oct. 2019, doi: 10.1016/j.nanoen.2019.103929.
- [56] S. Wang *et al.*, "A Novel Multi-Sulfur Source Collaborative Chemical Bath Deposition Technology Enables 8%-Efficiency Sb₂S₃ Planar Solar Cells," *Advanced Materials*, Oct. 2022, doi: 10.1002/adma.202206242.
- [57] M. Cao *et al.*, "Chemical bath deposition of SnS:Cu/ZnS for solar hydrogen production and solar cells," *J Alloys Compd*, vol. 863, May 2021, doi: 10.1016/j.jallcom.2021.158727.

- [58] S. I. Abbas, S. F. Hathot, A. S. Abbas, and A. A. Salim, "Influence of Cu doping on structure, morphology and optical characteristics of SnO₂ thin films prepared by chemical bath deposition technique," *Opt Mater (Amst)*, vol. 117, Jul. 2021, doi: 10.1016/j.optmat.2021.111212.
- [59] A. F. Abdulrahman, S. M. Ahmed, S. M. Hamad, and A. A. Barzinjy, "Effect of Growth Temperature on Morphological, Structural, and Optical Properties of ZnO Nanorods Using Modified Chemical Bath Deposition Method," *J Electron Mater*, vol. 50, no. 3, pp. 1482–1495, Mar. 2021, doi: 10.1007/s11664-020-08705-7.
- [60] S. M. Pawar, B. S. Pawar, J. H. Kim, O. S. Joo, and C. D. Lokhande, "Recent status of chemical bath deposited metal chalcogenide and metal oxide thin films," *Current Applied Physics*, vol. 11, no. 2. Elsevier B.V., pp. 117–161, 2011. doi: 10.1016/j.cap.2010.07.007.
- [61] B. A. Ezekoye, P. O. Offor, V. A. Ezekoye, and F. I. Ezema, "Chemical Bath Deposition Technique of Thin Films: A Review," *Int J Sci Res*, vol. 2, no. 8, pp. 452–456, 2013.
- [62] R. Zein and I. Alghoraibi, "Effect of Deposition Time on Structural and Optical Properties of ZnS Nanoparticles Thin Films Prepared by CBD Method," *Article in International Journal of ChemTech Research*, vol. 6, no. 5, pp. 3220–3227, 2014, [Online]. Available: <https://www.researchgate.net/publication/274252789>
- [63] P. K. Nair, P. Parmananda, and M. T. S. Nair, "Mathematical model simulating the growth of compound semiconductor thin films via chemical bath deposition," 1999.
- [64] Gary. Hodes, *Chemical solution deposition of semiconductor films*. Marcel Dekker, 2003.
- [65] E. Guneri, C. Ulutas, F. Kirmizigul, G. Altindemir, F. Gode, and C. Gumus, "Effect of deposition time on structural, electrical, and optical properties of SnS thin films deposited by chemical bath deposition," *Appl Surf Sci*, vol. 257, no. 4, pp. 1189–1195, Dec. 2010, doi: 10.1016/j.apsusc.2010.07.104.
- [66] A. Carrillo-Castillo, R. C. Ambrosio Lázaro, A. Jimenez-Pérez, C. A. Martínez Pérez, E. C. de La Cruz Terrazas, and M. A. Quevedo-López, "Role of complexing agents in chemical bath deposition of lead sulfide thin films," *Mater Lett*, vol. 121, pp. 19–21, Apr. 2014, doi: 10.1016/j.matlet.2014.01.088.
- [67] J. Liu, A. Wei, and Y. Zhao, "Effect of different complexing agents on the properties of chemical-bath-deposited ZnS thin films," *J Alloys Compd*, vol. 588, pp. 228–234, Mar. 2014, doi: 10.1016/j.jallcom.2013.11.042.
- [68] F. G. Hone and T. Abza, "Short review of factors affecting chemical bath deposition method for metal chalcogenide thin films," *International Journal of Thin Film Science and Technology*, vol. 8, no. 2. Natural Sciences Publishing, pp. 43–52, May 01, 2019. doi: 10.18576/ijtfst/080203.
- [69] Y. Rodríguez-Lazcano, Y. Peña, M. T. S. Nair, and P. K. Nair, "Polycrystalline thin films of antimony selenide via chemical bath deposition and post deposition treatments," *Thin Solid Films*, vol. 493, no. 1–2, pp. 77–82, Dec. 2005, doi: 10.1016/j.tsf.2005.07.238.

- [70] J. B. Mooney and S. B. Radding, "Spray Pyrolysis Processing," *Annual Review of Materials Science*, vol. 12, pp. 81–101, 1982, [Online]. Available: www.annualreviews.org
- [71] J. H. Saadie, "Influence of Thickness on Electrical and Optical Properties of Tellurium Thin Films Deposited by Chemical Spray Pyrolysis," *International Journal of Applied Mathematics, Electronics and Computers*, vol. 3, no. 2, p. 96, Feb. 2015, doi: 10.18100/ijamec.27133.
- [72] D. S. Boyle, A. Bayer, M. R. Heinrich, O. Robbe, and P. O'Brien, "Novel approach to the chemical bath deposition of chalcogenide semiconductors," *Thin Solid Films*, vol. 361–362, pp. 150–154, Feb. 2000, doi: 10.1016/S0040-6090(99)00789-0.
- [73] V. A. Volkovich *et al.*, "Substrate spacing and thin-film yield in chemical bath deposition of semiconductor thin films," *Semicond. Sci. Technol*, vol. 15, pp. 1022–1029, 2000, doi: 10.1088/0268-1242/15/11/302.
- [74] H. S. Nalwa, *Handbook of thin film materials*. Academic Press, 2002.
- [75] R. W. Johnson, A. Hultqvist, and S. F. Bent, "A brief review of atomic layer deposition: From fundamentals to applications," *Materials Today*, vol. 17, no. 5. Elsevier B.V., pp. 236–246, 2014. doi: 10.1016/j.mattod.2014.04.026.
- [76] V. M. Koch *et al.*, "Sb₂Se₃ Thin-Film Growth by Solution Atomic Layer Deposition," *Chemistry of Materials*, 2022, doi: 10.1021/acs.chemmater.2c01550.
- [77] S. Polivtseva *et al.*, "A novel thermochemical metal halide treatment for high-performance Sb₂Se₃ photocathodes," *Nanomaterials*, vol. 11, no. 1, pp. 1–14, Jan. 2021, doi: 10.3390/nano11010052.
- [78] X. Liu *et al.*, "Improving the performance of Sb₂Se₃ thin film solar cells over 4% by controlled addition of oxygen during film deposition," *Progress in Photovoltaics: Research and Applications*, vol. 23, no. 12, pp. 1828–1836, Dec. 2015, doi: 10.1002/pip.2627.
- [79] S. Yao *et al.*, "Improved Performance of Thermally Evaporated Sb₂Se₃ Thin-Film Solar Cells via Substrate-Cooling-Speed Control and Hydrogen-Sulfide Treatment," *ACS Appl Mater Interfaces*, vol. 12, no. 21, pp. 24112–24124, May 2020, doi: 10.1021/acsami.0c03674.
- [80] S. Rijal, D. B. Li, R. A. Awni, S. S. Bista, Z. Song, and Y. Yan, "Influence of Post-selenization Temperature on the Performance of Substrate-Type Sb₂Se₃ Solar Cells," *ACS Appl Energy Mater*, vol. 4, no. 5, pp. 4313–4318, May 2021, doi: 10.1021/acsaem.1c00657.
- [81] K. Shen *et al.*, "Efficient and Stable Planar n–i–p Sb₂Se₃ Solar Cells Enabled by Oriented 1D Trigonal Selenium Structures," *Advanced Science*, vol. 7, no. 16, Aug. 2020, doi: 10.1002/advs.202001013.
- [82] S. Rijal *et al.*, "Templated Growth and Passivation of Vertically Oriented Antimony Selenide Thin Films for High-Efficiency Solar Cells in Substrate Configuration," *Adv Funct Mater*, vol. 32, no. 10, Mar. 2022, doi: 10.1002/adfm.202110032.
- [83] Z. Li *et al.*, "9.2%-efficient core-shell structured antimony selenide nanorod array solar cells," *Nat Commun*, vol. 10, no. 1, Dec. 2019, doi: 10.1038/s41467-018-07903-6.

- [84] G. X. Liang *et al.*, "Sputtered and selenized Sb₂Se₃ thin-film solar cells with open-circuit voltage exceeding 500 mV," *Nano Energy*, vol. 73, Jul. 2020, doi: 10.1016/j.nanoen.2020.104806.
- [85] R. Tang *et al.*, "Heterojunction Annealing Enabling Record Open-Circuit Voltage in Antimony Triselenide Solar Cells," *Advanced Materials*, vol. 34, no. 14, Apr. 2022, doi: 10.1002/adma.202109078.
- [86] S. Chen *et al.*, "Recent progress and perspectives on Sb₂Se₃-based photocathodes for solar hydrogen production via photoelectrochemical water splitting," *Journal of Energy Chemistry*, vol. 67. Elsevier B.V., pp. 508–523, Apr. 01, 2022. doi: 10.1016/j.jechem.2021.08.062.
- [87] M. Wang, S. Wang, Q. Zhang, S. Pan, Y. Zhao, and X. Zhang, "Controlling the Crystallographic Orientation of Sb₂Se₃ Film for Efficient Photoelectrochemical Water Splitting," *Solar RRL*, vol. 6, no. 4, Apr. 2022, doi: 10.1002/solr.202100798.
- [88] Y. Zhang, Y. Zhang, H. Ma, Y. Feng, S. Wang, and Z. Li, "High-responsivity, self-driven visible-near infrared Sb₂Se₃ nanorod array photodetector," *Opt Express*, vol. 29, no. 24, p. 39549, Nov. 2021, doi: 10.1364/oe.442621.
- [89] C. Liu *et al.*, "A study on optical properties of Sb₂Se₃ thin films and resistive switching behavior in Ag/Sb₂Se₃/W heterojunctions," *Results Phys*, vol. 13, Jun. 2019, doi: 10.1016/j.rinp.2019.102228.
- [90] S. Rühle, "Tabulated values of the Shockley-Queisser limit for single junction solar cells," *Solar Energy*, vol. 130, pp. 139–147, Jun. 2016, doi: 10.1016/j.solener.2016.02.015.
- [91] "Sigma-Aldrich." <https://www.sigmaaldrich.com/EE/en> (accessed Nov. 18, 2022).
- [92] G. Cho, Y. Park, Y. K. Hong, and D. H. Ha, "Ion exchange: an advanced synthetic method for complex nanoparticles," *Nano Convergence*, vol. 6, no. 1. Korea Nano Technology Research Society, Dec. 01, 2019. doi: 10.1186/s40580-019-0187-0.
- [93] V. Shamraienko *et al.*, "Cation exchange on colloidal copper selenide nanosheets: A route to two-dimensional metal selenide nanomaterials," *J Mater Chem C Mater*, vol. 9, no. 46, pp. 16523–16535, Dec. 2021, doi: 10.1039/d1tc04815e.
- [94] H. S. Dong, S. M. Hughes, Y. Yin, and A. P. Alivisatos, "Cation exchange reactions in ionic nanocrystals," *Science (1979)*, vol. 306, no. 5698, pp. 1009–1012, Nov. 2004, doi: 10.1126/science.1103755.
- [95] J. B. Rivest and P. K. Jain, "Cation exchange on the nanoscale: An emerging technique for new material synthesis, device fabrication, and chemical sensing," *Chem Soc Rev*, vol. 42, no. 1, pp. 89–96, Dec. 2013, doi: 10.1039/c2cs35241a.
- [96] V. Lesnyak, R. Brescia, G. C. Messina, and L. Manna, "Cu Vacancies Boost Cation Exchange Reactions in Copper Selenide Nanocrystals," *J Am Chem Soc*, vol. 137, no. 29, pp. 9315–9323, Jul. 2015, doi: 10.1021/jacs.5b03868.
- [97] F. D. Ott, L. L. Spiegel, D. J. Norris, and S. C. Erwin, "Microscopic theory of cation exchange in CdSe nanocrystals," *Phys Rev Lett*, vol. 113, no. 15, Oct. 2014, doi: 10.1103/PhysRevLett.113.156803.

- [98] B. Bai *et al.*, "Semiconductor Nanocrystal Engineering by Applying Thiol- and Solvent-Coordinated Cation Exchange Kinetics," *Angewandte Chemie - International Edition*, vol. 58, no. 15, pp. 4852–4857, Apr. 2019, doi: 10.1002/anie.201807695.
- [99] Y. Justo, L. K. Sagar, S. Flamee, Q. Zhao, A. Vantomme, and Z. Hens, "Less is more. Cation exchange and the chemistry of the nanocrystal surface," *ACS Nano*, vol. 8, no. 8, pp. 7948–7957, Aug. 2014, doi: 10.1021/nn5037812.
- [100] T. Galle *et al.*, "Simultaneous Ligand and Cation Exchange of Colloidal CdSe Nanoplatelets toward PbSe Nanoplatelets for Application in Photodetectors," *Journal of Physical Chemistry Letters*, vol. 12, no. 21, pp. 5214–5220, Jun. 2021, doi: 10.1021/acs.jpcllett.1c01362.
- [101] C. J. Hibberd *et al.*, "Structural properties of Cu(In,Ga)Se₂ thin films prepared from chemically processed precursor layers." [Online]. Available: <https://dspace.lboro.ac.uk/>
- [102] A. O. Yalcin *et al.*, "Atomic resolution monitoring of cation exchange in CdSe-PbSe heteronanocrystals during epitaxial solid-solid-vapor growth," *Nano Lett*, vol. 14, no. 6, pp. 3661–3667, Jun. 2014, doi: 10.1021/nl501441w.
- [103] M. Casavola, M. A. van Huis, S. Bals, K. Lambert, Z. Hens, and D. Vanmaekelbergh, "Anisotropic cation exchange in PbSe/CdSe core/shell nanocrystals of different geometry," *Chemistry of Materials*, vol. 24, no. 2, pp. 294–302, Jan. 2012, doi: 10.1021/cm202796s.
- [104] H. Chen, C. Cao, B. Ge, Y. Li, J. Han, and Z. Chen, "Wafer-scale metal chalcogenide thin films: Via an ion exchange approach," *J Mater Chem C Mater*, vol. 8, no. 41, pp. 14393–14401, Nov. 2020, doi: 10.1039/d0tc03540h.
- [105] C. Bothe *et al.*, "Festkörperchemie auf der Nanoskala: Ionentransport über Zwischengitterplätze oder Leerstellen?," *Angewandte Chemie*, vol. 127, no. 47, pp. 14389–14393, Nov. 2015, doi: 10.1002/ange.201507263.
- [106] R. Tang, X. Y. Chen, G. X. Liang, Z. H. Su, J. ting Luo, and P. Fan, "Magnetron sputtering deposition and selenization of Sb₂Se₃ thin film for substrate Sb₂Se₃/CdS solar cells," *Surf Coat Technol*, vol. 360, pp. 68–72, Feb. 2019, doi: 10.1016/j.surfcoat.2018.12.102.
- [107] M. Leng *et al.*, "Selenization of Sb₂Se₃ absorber layer: An efficient step to improve device performance of CdS/Sb₂Se₃ solar cells," *Appl Phys Lett*, vol. 105, no. 8, Aug. 2014, doi: 10.1063/1.4894170.
- [108] V. Kumar *et al.*, "Analysis of Se Co-evaporation and Post-selenization for Sb₂Se₃-Based Solar Cells," *ACS Appl Energy Mater*, vol. 4, no. 11, pp. 12479–12486, Nov. 2021, doi: 10.1021/acsaem.1c02301.
- [109] P. Fan *et al.*, "Quasi-Vertically Oriented Sb₂Se₃Thin-Film Solar Cells with Open-Circuit Voltage Exceeding 500 mV Prepared via Close-Space Sublimation and Selenization," *ACS Appl Mater Interfaces*, vol. 13, no. 39, pp. 46671–46680, Oct. 2021, doi: 10.1021/acsaem.1c13223.
- [110] G. Jeong, S. Ji, J. Choi, J. Jung, and B. Shin, "Comprehensive rear surface passivation of superstrate Sb₂Se₃ solar cells via post-deposition selenium annealing treatments and the application of an electron blocking layer," *Faraday Discuss*, 2021, doi: 10.1039/d1fd00056j.

- [111] Thermo Fisher Scientific, "Principles of Scanning Electron Microscopy." <https://www.thermofisher.com/ee/en/home/materials-science/learning-center/applications/scanning-electron-microscope-sem-electron-column.html> (accessed Nov. 11, 2022).
- [112] Element, "X-Ray Diffraction Analysis (XRD)." <https://www.element.com/materials-testing-services/x-ray-diffraction> (accessed Nov. 16, 2022).
- [113] G. F. Harrington and J. Santiso, "Back-to-Basics tutorial: X-ray diffraction of thin films," *J Electroceram*, vol. 47, no. 4, pp. 141–163, Dec. 2021, doi: 10.1007/s10832-021-00263-6.
- [114] Mario. Birkholz, P. F. Fewster, and Christoph. Genzel, *Thin film analysis by X-ray scattering*. Wiley-VCH, 2006.
- [115] Horiba Scientific, "Raman Spectroscopy." <https://www.horiba.com/int/scientific/technologies/raman-imaging-and-spectroscopy/raman-spectroscopy/> (accessed Nov. 04, 2022).
- [116] Agilent, "UV-Vis Spectroscopy & Spectrophotometer FAQs." <https://www.agilent.com/en/support/molecular-spectroscopy/uv-vis-uv-vis-nir-spectroscopy/uv-vis-spectroscopy-spectrophotometer-basics> (accessed Nov. 05, 2022).
- [117] DeNovix, "What is a UV-Vis Spectrophotometer?" <https://www.denovix.com/blog/what-is-a-uv-vis-spectrophotometer/> (accessed Nov. 05, 2022).
- [118] B. P. Kafle, "Introduction to nanomaterials and application of UV-Visible spectroscopy for their characterization," in *Chemical Analysis and Material Characterization by Spectrophotometry*, Elsevier, 2020, pp. 147–198. doi: 10.1016/b978-0-12-814866-2.00006-3.
- [119] V. Saini *et al.*, "Structural and optoelectronic properties of P3HT-graphene composites prepared by in situ oxidative polymerization," in *Journal of Applied Physics*, Sep. 2012, vol. 112, no. 5. doi: 10.1063/1.4751271.
- [120] S. Polivtseva, N. Spalatu, A. Abdalla, O. Volobujeva, J. Hiie, and S. Bereznev, "Pulsed Laser Deposition of Zn(O,Se) Layers for Optoelectronic Application," *ACS Appl Energy Mater*, vol. 1, no. 11, pp. 6505–6512, Nov. 2018, doi: 10.1021/acsaem.8b01431.
- [121] X. Gong *et al.*, "In-situ micro-Raman study of SnSe single crystals under atmosphere: Effect of laser power and temperature," *Spectrochim Acta A Mol Biomol Spectrosc*, vol. 265, Jan. 2022, doi: 10.1016/j.saa.2021.120375.
- [122] A. Shongalova, M. R. Correia, B. Vermang, J. M. V. Cunha, P. M. P. Salomé, and P. A. Fernandes, "On the identification of Sb₂Se₃ using Raman scattering," *MRS Commun*, vol. 8, no. 3, pp. 865–870, Sep. 2018, doi: 10.1557/mrc.2018.94.
- [123] N. Fleck *et al.*, "Identifying Raman Modes of Sb₂Se₃ and their Symmetries using Angle-Resolved Polarised Raman Spectra †", doi: 10.1039/cXCP00000x/fig.
- [124] M. Kumar, S. Rani, Y. Singh, K. S. Gour, and V. N. Singh, "Tin-selenide as a futuristic material: properties and applications," *RSC Advances*, vol. 11, no. 12. Royal Society of Chemistry, pp. 6477–6503, Feb. 03, 2021. doi: 10.1039/d0ra09807h.